SUBERMAN Regulates Developmental Suberization of the Arabidopsis Root Endodermis

PROFESSOR SHUANG WU (Orcid ID : 0000-0003-1913-8125)

DR ASAPH AHARONI (Orcid ID : 0000-0002-6077-1590)

Article type : Original Article

SUBERMAN Regulates Developmental Suberization of the Arabidopsis Root Endodermis

Hagai Cohen[1], Vadim Fedyuk[1], Chunhua Wang[2], Shuang Wu[2], Asaph Aharoni[1,*]

[1]Department of Plant and Environmental Sciences, Weizmann Institute of Science, Rehovot 7610001, Israel

[2]FAFU-UCR Joint Center and Fujian Provincial Key Laboratory of Haixia Applied Plant Systems Biology, Fujian Agriculture and Forestry University, Fuzhou 350002, China

[*]**Corresponding author e-mail address:** asaph.aharoni@weizmann.ac.il

Running Head: Root Endodermis Suberization

This article has been accepted for publication and undergone full peer review but has not been through the copyediting, typesetting, pagination and proofreading process, which may lead to differences between this version and the Version of Record. Please cite this article as doi: 10.1111/TPJ.14711

ABSTRACT

Root endodermis, the innermost cortical layer surrounding the root vasculature, serves as the foremost barrier to water, solutes, and nutrients taken up from soil. Endodermis barrier functionality is achieved via its hydrophobic coating of lignified Casparian strips and the suberin lamellae; nonetheless the regulatory mechanisms underlying endodermis suberization are still elusive. Here, we discovered that the Arabidopsis SUBERMAN (SUB) transcription factor controls establishment of the root suberin lamellae. Transient expression of SUB in *Nicotiana benthamiana* (*N. benthamiana*) leaves resulted in the induction of heterologous suberin genes, the accumulation of suberin-type monomers, and consequent deposition of suberin-like lamellae. We demonstrate that SUB exerts its regulatory roles by transactivating promoters of suberin genes. In Arabidopsis, SUB is expressed in patchy and continuous suberization root endodermal cells, and thus roots with higher or lower expression of SUB display altered suberin polymer deposition patterns and modified composition. While these changes did not interfere with Casparian strip formation they had a substantial effect on root uptake capacity resulting in varied root and leaf ionomic phenotypes. Gene expression profiling revealed that SUB function impacts transcriptional networks associated with suberin, phenylpropanoids, lignin and cuticular lipid biosynthesis, as well as root transport activities, hormone signaling and cell wall modification. Our findings highlight SUB as a regulator of root endodermis suberization during normal development, and its characterization is thus a key step towards dissecting the molecular mechanisms partaking in root endodermal barrier functionalities.

INTRODUCTION

Lipophilic barriers allow plants to thrive in terrestrial habitats as they minimize their water loss, facilitate exchange of gases and solutes, and protect them against environmental cues (Cohen et al., 2017). Suberin, one such barrier, is a heteropolymer consisting of polyaliphatic and polyphenolic domains (SPAD and SPPD, respectively). The spatial and temporal coordination of both domains is essential for the proper establishment of a complete suberin lamellae (Bernards 2002). SPAD is mainly composed of a mixture of very-long-chain C20 to C26 fatty acids, primary alcohols and glycerol (Beisson et al., 2012; Franke et al., 2005); while SPPD is mostly made up of hydroxycinnamic acid derivatives derived from the phenylpropanoid pathway (Bernards et al., 1995; Bernards and Razem 2001). Suberin forms a typical lamellar structure deposited in-between the plasma membrane and the cell wall of specialized tissues as tree bark, seed coat, skin of potato tubers, and russeted and/or reticulated fruit species like apple, pear, quince, and melon (Schreiber 2010; Cohen et al., 2019).

To date, a set of biosynthetic enzymes was shown to partake suberin metabolism, mostly in Arabidopsis. These include KCS2 and KCS20, *β*-ketoacyl-CoA synthases that generate primary very-long-chain fatty acids (Franke et al., 2009; Lee et al., 2009); GPAT5, a glycerol-3-phosphate acyltransferase producing monoacylglycerol esters (Beisson et al., 2007; Li et al., 2007b); ASFT, an aliphatic suberin feruloyl transferase catalyzing the acyl transfer from feruloyl-CoA to ω-hydroxy acids and fatty alcohols (Gou et al., 2009; Molina et al., 2009); CYP86A1 and CYP86B1, two cytochrome P450 oxidases accounting for ω-hydroxy acid biosynthesis (Hofer et al., 2008; Compagnon et al., 2009), as well as FAR1, FAR4 and FAR5, fatty acyl-CoA reductases that produce primary fatty alcohols (Wishwanath et al., 2013; Domergue et al., 2010). The ATP-binding cassette G proteins ABCG2, ABCG6 and ABCG20 as well as GLYCOSYLPHOSPHATIDYLINOSITOL-ANCHORED LIPID TRANSFER PROTEIN (LTPG15) were suggested to transport suberin monomers across the plasma membrane (Yadav et al., 2014; Lee and Suh 2018). Despite recent progress in our knowledge of suberin biosynthesis, relatively less data vis-à-vis the regulatory networks controlling suberin production is available. To date, seven regulators were associated with

the suberization processes: MYB41, is capable of inducing the deposition of suberin-like lamellae in leaf tissues of *Nicotiana benthamiana* and Arabidopsis (Kosma et al., 2014); MYB107 and MYB9 homologs were identified as positive regulators of suberin in the Arabidopsis seed coat (Lashbrooke et al., 2016); the NAC46 transcription factor was recently proven to play an important role in promoting suberin biosynthesis in Arabidopsis roots (Mahmood et al., 2019); MYB1 from cork oak (*Quercus suber*) that directly targets genes involved in suberin and lignin pathways (Capote et al., 2018); the potato (*Solanum tuberosum*) NAC103 found to negatively regulate periderm suberin in the tuber skin (Verdaguer et al., 2016) and the apple (*Malus x domestica*) MYB93 shown to partake the formation of suberized russeted skin during fruit development (Legay et al., 2016). The root endodermis is a renowned tissue that encompasses specialized suberin lamellae during its development, yet, no regulators of this vital process were reported thus far.

Root endodermis is the innermost cortical layer surrounding the root vasculature (Schreiber et al., 1999), serving as the primary barrier of water, solutes and nutrients that are taken up from the soil by roots before entering the stele and further distributed towards other plant organs. Endodermis barrier functionality is achieved by deposition of two hydrophobic polymers, lignin and suberin. Lignin builds the Casparian strips, ring-like structures encircling the walls of endodermal cells once these mature and fully elongate (Anderson et al., 2015; Barberon et al., 2016). The suberin lamellae appear at later stages of endodermis differentiation and are deposited in the inner side of their walls sealing it surface (Franke and Schreiber 2007). At early differentiation stages, endodermal cells are often suberized intermittently leading to ‘patchy suberization’ zone, while fully-differentiated mature endodermal cells form a zone of ‘continuous suberization’ (Barberon 2017). In the Arabidopsis root, Casparian strips are non-suberized and made of lignin. This explains why roots that are devoid of any detectable suberin can still establish and maintain functional Casparian strips (Naseer et al., 2012; Barberon et al., 2016). Casparian strips function as apoplastic barriers thereby preventing solute movement into the vasculature through the apoplast, but also from inner stele cells towards the cortex (Hosmani et al., 2013; Pfister et al., 2014; Kamiya et al., 2015). The suberin lamellae, however, limit transport via the

transcellular pathway (Barberon 2017). Together, these findings advocate that the two fundamental processes of endodermis (i.e. lignification and suberization) might be regulated separately in a spatiotemporal manner. Our understanding of the regulatory networks involved in Casparian strip formation has been progressively increasing (Roppolo et al., 2011; Kamiya et al., 2015; Liberman et al., 2015; Di Laurenzio et al., 1996; Helariutta et al., 2000; Heidstra et al., 2004; Sozzani et al., 2010; Cui et al., 2007), nevertheless, our knowledge of how endodermal cells undergo suberization and the regulatory mechanisms underlying this process remain indefinite.

Here, we discovered that the Arabidopsis SUBERMAN (SUB), a MYB-type transcription factor (i.e. MYB39), is a positive regulator of suberin deposition in the root endodermis layer. Transient expression of SUB in *Nicotiana benthamiana* (*N. benthamiana*) leaves resulted in the induction of heterologous suberin genes, the accumulation of suberin-type monomers, and consequent deposition of suberin-like lamellae. It appeared that SUB controls the expression of suberin genes by transactivating their promoters. We demonstrate that SUB operates primarily in the Arabidopsis root endodermis coinciding with archetypal expression patterns of suberin biosynthetic genes and the accumulation of suberin monomers. In accordance with this, roots with altered *SUB* expression exhibited substantial changes in their suberin profiles. Modified transcriptional programs associated with metabolism of phenylpropanoids, suberin, lignin and cuticular lipids, as well as those related to root transport activities and cell wall modification accompanied these changes. We found that these changes had a significant impact on root transport and uptake capacities resulting in varied root and leaf ionomic phenotypes. Notably, these did not seem to interfere with the formation of endodermis Casparian strips. Altogether, our work signifies SUB as a so far undisclosed transcription factor controlling suberin biosynthesis and moreover underscores the developmental plasticity of root endodermis as an apoplastic checkpoint for water and nutrients.

RESULTS

Transient expression of *SUBERMAN* induces the accumulation of suberin and the deposition of suberin-like lamellae in *N. benthamiana* leaves

We previously found that MYB107 and MYB9 homologs promote suberin biosynthesis in the Arabidopsis seed coat (Lashbrooke et al., 2016). Together with the Arabidopsis MYB93, MYB92, MYB53 and MYB39, as well as homologous proteins from other species (*e.g.* the tomato and potato MYB93; apple MYB53 and grape MYB107), these factors are positioned in either one of two previously defined subgroups of MYB-type proteins (Dubos et al., 2010). Among these proteins, MYB39, MYB107 and MYB9 contain three highly conserved *C*-terminal protein motifs (Supplemental Figure 1). We thus postulated that MYB39 (termed here SUBERMAN; SUB) might function as a regulator of suberin biosynthesis.

Leaves do not produce suberin and their epidermal surfaces are covered by a typical cuticle layer made predominantly from cutin and waxes. Therefore, to assess whether SUB could induce lamellar deposition of suberin we transiently agroinfiltrated *N. benthamiana* leaves with a vector overexpressing its coding sequence (i.e. SUB-OX) and compared them to leaves infiltrated with an empty vector control (i.e. EV). Following validation of *SUB* expression in agroinfiltrated regions (Supplemental Figure 2), epidermal and mesophyll cells from ultrathin leaf sections were examined for cell wall structure by Transmission Electron Microscope (TEM). The analysis revealed the occurrence of unique suberin-like lamellae deposited in between the plasma membrane and the inner side of the primary cell walls of both epidermal and mesophyll cells of leaves expressing the SUB-OX vector. These structures, however, could not be detected in cells of control leaves (Figure 1A). Additionally, the cuticle layer of SUB-OX epidermal cells appeared thinner (Figure 1A). Together, these observations imply that SUB expression can induce *de novo* formation of suberin in leaves.

Chemical analysis of leaf polyester composition following infiltration with the SUB-OX vector demonstrated the accumulation of characteristic suberin-type components along with cutin monomers normally present in leaves (Figure 1B). Significant increase was detected in the case of the hydroxycinnamic acids coumarate and caffeate, and particularly ferulate, the

most abundant aromatic compound in suberin (668-fold increase in SUB-OX leaves) (Figure 1B). We also detected higher levels of very long-chain C20-C24 fatty acids, C16 and C20-C24 primary fatty alcohols, C20-C22 ω-hydroxy fatty acids, together with the accumulation of dominating suberin-type monomers C18:1 and C18:2 ω-hydroxy fatty acids and C16, C18, C18:1 and C22 dicarboxylic acids, all providing solid chemical fingerprint for the deposition of suberin. Typical cutin monomers such as long-chain C16 fatty acid, C16 ω-hydroxy fatty acid, as well as cutin most dominant monomer - 10(9),16-dihydroxy fatty acid, also displayed higher levels in SUB-OX as compared to EV leaves (Figure 1B). The accumulation of suberin was limited to leaf sections expressing SUB-OX, as adjacent non-infiltrated regions of these leaves displayed similar polyester composition as found in EV infiltrated leaves (Supplemental Figure 3). Together, the analysis showed that transient expression of SUB in *N. benthamiana* leaves led to an increased flux of acyl-lipids and phenylpropanoid aromatic compounds towards the biosynthesis of suberin.

The deposition of suberin lamellae in SUB-OX leaves was accompanied by induced expression of putative *N. benthamiana* homolog genes involved in the biosynthesis, transport and regulation of suberin. For example, the increase in all detected ω-hydroxy fatty acids was accompanied by 405- and 182-fold elevations in *CYP86A1* and *CYP86B1* gene transcripts, respectively, that are critical for ω-hydroxylation of fatty acids (Figure 1C). Similarly, *FAR1*, *FAR4* and *FAR5* were induced in SUB-OX leaf sections in agreement with the increased amount of primary fatty alcohols, particularly of long-chain lengths (Figure 1C). *KCS2* and *KCS20* that provide primary very-long-chain fatty acids for suberin biosynthesis displayed elevated expression, together with *GPAT5*, a key suberin biosynthetic enzyme. The marked accumulation of ferulate in SUB-OX leaves was accompanied by 77-fold elevated expression of *ASFT* that uses feruloyl-CoA supplied by the core phenylpropanoid pathway to generate ω-hydroxyalkyl and *n*-alkyl ferulate suberin monomers. Furthermore, the expression of putative *N. benthamiana* suberin regulators homologs, i.e., *MYB107*, *MYB9*, *MYB41* and *MYB39* (*SUB*) itself were induced (Figure 1C). On the other hand, no changes were detected in the expression of two key cuticle biosynthetic genes, *CER1* and *CER7* (Bernard et al., 2012), as well as of *ABCG11* encoding a membrane-localized ATP-

binding cassette transporter required for cutin transport to the extracellular matrix (Panikshvili et al., 2007). These findings implied that SUB affects the expression of genes in the suberin pathway rather than those involved in cuticle formation.

The highly-conserved phenylpropanoid pathway supplies the hydroxycinnamic acid derivatives essential for SPPD assembly. We therefore analyzed the expression of key genes operating in this pathway and revealed that most of them displayed significantly induced expression in SUB-OX leaves. This set of genes included *PAL1* (*PHENYLALANINE AMONIA-LYASE1*), *4CL* (*4-COUMARATE:COA LIGASE*), *HCT* (*HYDROXYCINNAMOYL-COA SHIKIMATE/QUINATE HYDROXYCINNAMOYL TRANSFERASE*), *C3H* (*p-COUMARATE 3-HYDROXYLASE*), *CCoAOMT* (*CAFFEOYL COENZYME A ESTER O-METHYLTRANSFERASE*), *F5H* (*FERULIC ACID 5-HYDROXYLASE*) and *COMT* (*CAFFEATE O-METHYLTRANSFERASE*) (Figure 1C). Interestingly, we did not detect a change in the expression of *CAD5* (*CINNAMYL ALCOHOL DEHYDROGENASE 5*) that carries out the final NADPH-dependent reduction of hydroxycinnamaldehydes to their respective monolignols characteristic to lignin (Figure 1C). This implies that overexpression of SUB caused the induced expression of phenylpropanoid genes important to SPPD, but not those essential to lignin monomer synthesis.

SUB is expressed in endodermal cells displaying patchy and continuous suberization

We next examined in which Arabidopsis plant tissues *SUB* is expressed. For that, we generated promoter-reporter lines where the *SUB* gene 5' upstream region (~3000 bp) was fused to an RFP reporter (i.e. pSUB::RFP) and analyzed them under Confocal Laser Scanning Microscope (CLSM). Observing 10-day-old pSUB::RFP seedlings revealed substantial RFP signals in endodermal cells possessing patchy and continuous suberization along the root axis. Yet, no signal could be detected in non-suberized root zones of the same roots (Figure 2A). Such developmental- and tissue-specific expression pattern of *SUB* coincides with previous reports showing the deposition patterns of suberin during the Arabidopsis root development. They also match the endodermis-specific expression of reporter proteins driven by upstream regions of the *GPAT5*, *CYP86A1* and *CYP86B1*, three

suberin key biosynthetic genes (Supplemental Figure 4). Thus, the results up to here propose an association between SUB and the regulation of endodermis suberization. Infiltration experiments in *N. benthamiana* leaves validated that the SUB transcription factor localizes to the nucleus (Figure 2B).

Roots with altered *SUB* expression display changes in suberin profiles

In order to study the effect of altered *SUB* expression on root endodermis suberization, we characterized a *SUB* mutant with 87% reduced *SUB* expression in roots, and generated plants with approximately 37-fold increased root *SUB* expression (i.e. SUB-OX) (Supplemental Figure 5). We observed suberin patterns in 5-day-old roots by staining with fluorol yellow (FY); a fluorescent dye capable of indicating the presence of lamellar suberin but not diffused non-lamellar suberin (Lux et al., 2005; Ursache et al., 2018). As expected, WT roots displayed strong staining in continuous suberization zones, sporadic staining patterns within patchy suberization zones, and no staining in the non-suberized zones (Figure 3A). *sub* roots exhibited weaker staining patterns in both patchy and continuous suberization zones as compared to those of WT roots (Figure 3A). However, SUB-OX roots displayed remarkable ectopic suberin staining in endodermal, cortical and epidermal cells, where staining patterns in the epidermis seem less intense than those observed in the endodermis and cortex (Figure 3A). The ectopic suberization was observed in both patchy and continuous suberization zones of SUB-OX roots with even some staining patterns of suberin detected in endodermal cells located in lower root zones that naturally do not undergo suberization (Figure 3A). Ectopic suberization was previously demonstrated to occur as a compensative response in roots of several mutant plants harboring defective Casparian strips due to altered expression of different Casparian strip genes (e.g. *esb-1*, *casp1casp3*, *myb36-1*) (Kamiya et al., 2015; Hosmani et al., 2013). However, CLSM analyses of Casparian strip autofluorescence revealed no apparent change in their appearance in non-suberized, patchy or continuous suberized zones of WT, *sub* and SUB-OX roots (Supplemental Figure 6). Hence, these observations implicated that the striking perturbations in suberin lamellae of *sub* and SUB-OX roots did not compromise Casparian

strip formation, and that the activity of SUB in roots is confined to the establishment of the suberin lamellae.

To further investigate the timing of suberin deposition, we calculated differences in the onset of suberization along the root axis by counting the percentage of endodermal cells showing no suberization, patchy suberization or continuous suberization, as previously defined (Barberon et al., 2016). Roots of the *sub* mutant displayed delayed suberization with more endodermal cells possessing patchy suberization and less cells displaying continuous suberization, as compared to WT ones (Figure 3B). In contrast, SUB-OX roots entered the stage of continuous suberization much earlier than WT and *sub* roots, and displayed much less endodermal cells with patchy or no suberization at all (Figure 3B).

The above findings suggested considerable modifications in the deposition patterns of endodermis suberin lamellae of *sub* and SUB-OX roots. To test this, we carried out TEM analysis of ultrathin sections dissected from continuous suberization root zones of 10-day-old seedlings of the three genotypes. Genuine suberin lamellae was detected in the inner side of endodermal cell walls of WT roots along with a typical thick primary cell walls of cortical and epidermal cells lacking a suberin lamellae (Figure 3C). The suberin layer in the endodermis of *sub* root, however, appeared thinner and contained fewer visible lamellae. As in the case of WT roots, normal primary cell walls were detected in cortical and epidermal cells of *sub* roots with no visible suberin lamellae structure (Figure 3C). In accord with FY-staining of suberin, ectopic deposition of distinct suberin lamellae was detected in cortical cell walls of SUB-OX roots, alongside the endodermis lamellae (Figure 3C). Lamellar structures could also be detected in the epidermal cell walls of SUB-OX roots; however, it appears to be thinner with less observable lamellae (Figure 3C).

To examine changes in suberin composition between the genotypes, we analyzed their root polyester profiles. We found a significant 2.2-fold decrease in total suberin content in *sub* mutant roots and 2.4-fold elevation in SUB-OX roots. The reductions in *sub* roots included lower levels of the aromatic components ferulate and coumarate, very-long-chain C22-C24 fatty acids, C18-C22 fatty alcohols, C16, C18:1, C20, C22 and C24 ω-hydroxy acids, and in C18:1 dicarboxylic acid (Figure 3D). Conversely, SUB-OX roots accumulated

large amounts of essentially almost all detected suberin monomers as compared to WT roots (Figure 3D). Among those, ferulate and coumarate exhibiting 3 and 5-fold higher levels, very-long-chain C22 and C24 fatty acids with 2.7- and 5.2-fold changes, C22 fatty alcohol by 3.5-fold, C22 and C24 ω-hydroxy acids by 4.2- and 8.1-fold changes, and C18:1 and C22 dicarboxylic acids by 2.8- and 8.3-fold changes (Figure 3D). Overall, the findings described above provided several lines of evidence that alteration of *SUB* expression in roots has substantial effect on suberin profiles. Overexpression of *SUB* led to enhanced accumulation of suberin not only in the endodermis of SUB-OX roots, but also in other root cell layers and zones that do not deposit suberin lamellae under normal development. On the other hand, lower expression of *SUB* in mutant roots resulted in lower accumulation of suberin particularly in their endodermal cells.

SUB transactivates upstream regions of genes acting in suberin biosynthesis, transport and pathway regulation

The results up to here suggest that SUB can activate the expression of suberin-associated genes and capable of triggering their transcription outside the endodermis boundaries in cell layers that naturally do not produce suberin. To test this, we utilized two approaches: (i) using promoter-reporter lines in which the native 5' upstream regions of the *GPAT5*, *CYP86A1* and *CYP86B1* genes were fused to GUS and GFP (i.e. pGPAT5::NLS-GFP-GUS, pCYP86A1::NLS-GFP-GUS and pCYP86B1::NLS-GFP-GUS; Naseer et al, 2012) and transforming them with the SUB-OX vector; and (ii) performing transactivation in *N. benthamiana* (McNabb et al., 2005) to survey SUB capacity to activate reporter expression from upstream regions (putative promoters) of representative Arabidopsis suberin genes.

Using CLSM we examined the expression patterns *GPAT5*, *CYP86A1* and *CYP86B1* suberin biosynthetic genes in continuous suberization root zones of their three reporter lines. The revealed the expected endodermis-specific expression of the three of them (Figure 4A). Markedly, when the pGPAT5::NLS-GFP-GUS reporter line was transformed with the SUB-OX vector, we could detect a significant enhancement of *GPAT5* expression within endodermal cells, but also in cortical and epidermal cells (Figure 4A). Enhanced expression

of *CYP86A1* and *CYP86B1* could also be detected in the endodermis of the pCYP86A1::NLS-GFP-GUS and pCYP86B1::NLS-GFP-GUS reporter lines expressing SUB-OX. Yet, it was confined to the endodermis cell layer with no apparent ectopic expression in cortical and epidermal cells (Figure 4A).

Transactivation assay was done by co-infiltrating *N. benthamiana* leaves with either the SUB-OX or EV control vectors, together with reporter constructs of ten Arabidopsis suberin genes containing their 5' upstream regions (putative promoters; Supplemental Figures 7 and 8). It appeared that SUB can transactivate suberin gene promoters to varying degrees. The highest transactivation levels were observed for the promoters of *GPAT5* and *ASFT* (the two predominant suberin biosynthetic genes) involved in aliphatic and aromatic monomer biosynthesis) and *CYP86B1* (involved in ω-hydroxy acid monomer biosynthesis), displaying 338-, 291- and 317-fold inductions, respectively (Figure 4B). Promoters of the suberin monomer transporter *ABCG6*, as well as of *FAR1* and *FAR4* genes involved in alcohol monomer biosynthesis, were induced by 9.3-, 4.5- and 2.4-folds, respectively (Figure 4B). SUB could also transactivate the promoters *MYB107* and *MYB41* (~2.5-fold inductions for both regulators) but not of *MYB9* nor its own promoter (Figure 4B). Altogether, both assays provided evidence that SUB regulates suberin polymer formation and supports the changes in suberin profiles and deposition patterns observed in *sub* and SUB-OX roots.

Root uptake and transport capacities are perturbed in *sub* and SUB-OX plants

As mentioned before, the suberin lamellae seals the endodermis cells following the formation of Casparian strips, and affect the transcellular transport pathway throughout the root (Barberon 2017). We aimed at investigating whether the perturbed suberin lamellae in *sub* and SUB-OX roots affect their capacity to uptake and transport the two fluorescent tracers of PI and fluorescein diacetate (FDA). Five minutes post tracer application, PI was observed in WT only epidermal and cortical root cells (Figure 5A). A relatively similar phenomena was detected in *sub* roots, however, they exhibited much stronger staining patterns and fluorescence intensities (Figure 5A). In contrast, much lower intensities were measured in SUB-OX roots in which PI was mainly detected in lateral roots, epidermis, and

cortex, with only very weak virtual staining signals in the endodermis and Casparian strips (Figure 5A). This was likely since PI penetration was blocked already by the heavily-suberized walls of the epidermal and cortical cells of SUB-OX roots.

An additional time-course assay monitoring FDA uptake during 15 minutes corroborated the changes detected in the PI penetration assay. Two minutes following application, we detected FDA mainly in the epidermis of WT and SUB-OX roots, yet, it already accumulated to high levels in the epidermal and cortical cells of *sub* roots (Figure 5B). From this point onwards, FDA was gradually dissociated into WT root cortical cells (Figure 5B). Up to 15 minutes, the strong FDA buildup observed after 2 minutes in epidermal and cortical cells of *sub* roots consistently and rapidly dissociated into its inner root cell layers (Figure 5B). Yet, in SUB-OX roots, FDA was highly abundant in epidermal cells even after 15 min, with only trace signals detected in its cortical and endodermal cells (Figure 5B).

The above findings suggested that uptake capacities in *sub* and SUB-OX roots was malfunctioning as compared to WT. To test this further, we grew the roots of the three genotypes and WT on a soil medium mixed with vermiculite to ensure sufficient aeration while encouraging proper water drainage. We then harvested roots and rosette leaves from 3-week-old seedlings and profiled their elemental composition using Inductively Coupled Plasma-Mass Spectrometry (ICP-MS). Despite the lower amount of suberin and disrupted suberin lamellae, *sub* roots showed no significant change in the abundance of any of the detected elements as compared to WT roots. Nevertheless, *sub* rosette leaves displayed minor, yet significant increases of P, K, Rb and Sr levels (Figure 5C and Supplemental Table 1). In the case of SUB-OX plants, we detected substantially modified elemental profiles of both their roots and rosette leaves. Mg, K, Fe and Co were significantly lower in both tissues compared to their WT counterparts. Additionally, SUB-OX rosette leaves displayed lower abundances of Li, P, S, Ca, Mn, Cu, Rb and Sr (Figure 5C and Supplemental Table 1).

Transcriptome analysis reveals a tight link between SUB activity and root metabolism of suberin, phenylpropanoids and cuticular lipids

To identify genes potentially regulated by SUB, we carried out transcriptome analysis of WT, *sub* and SUB-OX roots. Principal Component Analysis (PCA) plot calculated from all expressed genes revealed clear differences between the three genotypes (Figure 6A), followed by differential expression algorithms [$|\log_2$ fold change$|$ > 1; false discovery rate (FDR) < 0.05] detecting 468 genes that were upregulated or downregulated in *sub* roots and 426 genes in SUB-OX (Supplemental Tables 2 and 3). Among these, 76 genes were shared between the two differentially expressed gene datasets (Figure 6B). Twenty three out of the 76 common genes displayed inverse expression in *sub* roots as compared to SUB-OX (i.e. lower in *sub* and higher in SUB-OX or *vice versa*), while 53 genes displayed similar expression pattern in the two genotypes (i.e. lower in *sub* and SUB-OX or higher in both of them) (Figure 6B).

The lion's share of genes in the *sub* set exhibited reduced expression compared to WT roots (133 and 335 upregulated and downregulated, respectively). These included lower expression of core phenylpropanoid genes such as *PAL1*, *4CL3* and *F3H* in accordance with lower suberin monomer levels in *sub* that partial depends on aromatic substrates delivered by the phenylpropanoid pathway. Moreover, numerous cell wall-associated genes displayed lower expression in *sub* including ones involved in modifying cell wall properties, such as *EXPANSIN* (*EXP*), *EXTENSIN* (*EXT*), *XYLOGLUCAN ENDOTRANSGLUCOSYLASE/HYDROLASE* (*XTH*), *ROOT-HAIR SPECIFIC* (*RHS*) and *CELLULOSE SYNTHASE-LIKE* (*CSL*). Apparently, these modifications were accompanied by changes in genes associated with signaling and regulatory pathways of abscisic acid (ABA), ethylene, auxin and jasmonic acid, as expression of many key factors involved in these hormonal processes was downregulated in *sub* roots (Supplemental Table 2). More genes included in the SUB-OX subset were upregulated as compared to *sub* roots (231 and 195 upregulated and downregulated, respectively). In contrast to transcriptome changes in *sub*, SUB-OX roots exhibited induced expression of phenylpropanoid and lignin genes including *LAC7, LAC13*, *CAFFEOYL COENZYME A ESTER O-METHYLTRANSFERASE* (*CCoAOMT*), *REDUCED EPIDERMAL FLUORESCENCE 1* (*REF1*) and *CINNAMYL-CoA REDUCTASE 2* (*CCR2*), *FERULOYL-CoA HYDROXYLASE 1* (*F6'H1*) and others.

Noticeably, elevated expression was also detected in a set of genes involved the biosynthesis of cuticular lipids [*LONG-CHAIN ACYL-CoA SYNTHETASES 2* and *9* (*LACS2*, *LACS9*), *3-KETOACYL-CoA SYNTHASE 1* (*KCS1*), *KETOACYL REDUCTASE* (*KCR*), *GLYCEROL-3-PHOSPHATE sn-2-ACYLTRANSFERASE* 4, 6 and 7 (*GPAT4*, *GPAT6, GPAT7*), *ECCERIFERUM 10* and *26* (*CER10, CER26*), cytochrome P450s *CYP86A2* and *CYP86A8*, as well as *FATTY ALCOHOL:CAFFEOYL-CoA CAFFEOYL TRANSFERASE* (*FACT*)], further implicating modifications in cell wall structure occurring in SUB-OX roots. We also detected altered expression of dozens of transporters and plasma membrane efflux carriers, including those encoding putative transporters of sugars (e.g. myoinositol and sucrose), organic acids (e.g. malate, fumarate and glutamate), and of micro- and macro-elements (e.g. nitrate, sulfur, zinc, aluminum and boron) (Supplemental Table 3). These findings provided a consistent explanation for the disordered uptake capacity observed in these roots.

The 76 genes that were common between *sub* and SUB-OX differentially expressed gene sets likely represent the core transcriptional gene expression programs associated with SUB activity. Functional annotation of these genes showed that SUB activity could be largely associated with the metabolism of suberin, phenylpropanoids, very-long-chain-fatty-acid (VLCFA)-CoA, lipids, as well as with phosphate starvation, stress response, ion binding and homeostasis, membrane transport and oxidoreduction activities (Supplemental Figure 9). Among the 23 genes showing inverse expression between the *sub* and SUB-OX sets, 21 were upregulated in SUB-OX but significantly downregulated in *sub* roots: 13 suberin-related genes (*KCS2*, *GPAT5*, *ASFT*, *CYP86A1*, *CYP86B1*, *FAR1*, *FAR4*, *FAR5*, *ABCG2*, *ABCG6*, *ABCG20*, *MYB41, SUB*); one lignin gene (*LAC5*); two genes involved in lipid and wax pathways (*CYP86A2*, *Pollen Ole e 1*); and additional 5 genes with unknown function. Only two genes with unknown function showed higher expression in *sub* roots but lower in SUB-OX (Figure 6C). The majority of the other 53 common genes displaying similar expression pattern (9 upregulated and 44 downregulated) in both genotypes relate with cell wall-modifications, transport of ions, phosphate homeostasis, oxidoreduction and phosphorylation activities, as well as hormonal signaling (Figure 6D). Additional interesting

subset of genes displaying repressed expression in both genotypes were those involved in the biosynthesis of lignin, lipids, sulfolipids, thalianols, and carbohydrates (Figure 6D). Overall, transcriptome profiling suggested a tight link between SUB activity and suberin metabolism, together with a strong, likely indirect effect on various aspects of root physiology such as uptake capacity, cell wall integrity and primary and secondary metabolism.

DISCUSSION

The findings of this study underscore the SUB transcription factor as a key mediator of suberin metabolism in plants, particularly of developmental endodermis suberization in the Arabidopsis root. Several key results support this view including (1) the formation of complete suberin lamellae in *N. benthamiana* leaves transiently expressing SUB-OX; (2) the ability of SUB to transactivate 5' upstream promoter regions of suberin biosynthesis, transport and regulatory genes; (3) *SUB* expression in patchy and continuous suberization endodermis root zones overlapping with typical spatiotemporal patterns of suberin gene expression and monomer accumulation; (4) the ectopic deposition of suberin lamellae outside endodermis boundaries in SUB-OX roots; and (5) the transcriptomic data displaying a tight link between SUB regulatory activities and the metabolism of suberin and phenylpropanoids.

SUBERMAN triggers the production of suberin and the deposition of suberin lamellae

Our knowledge of the regulatory mechanisms underlying suberin biosynthesis is limited. To date, several transcription factors were shown to associate with suberin metabolism. For example, overexpression of *AtMYB41* resulted in ectopic deposition of suberin lamellae in *N. benthamiana* leaves that accumulated 22-times more suberin-type than cutin-type aliphatic monomers (Kosma et al., 2014). Similarly, agroinfiltration of *MdMYB93* in *N. benthamiana* leaves yielded massive accumulation of suberin and remobilized phenylpropanoids towards its biosynthesis (Legay et al., 2016), and AtMYB107 and QsMYB1 were shown to activate

promoter regions of suberin biosynthesis genes (Gou et al., 2017; Capote et al., 2018). These chemical and transcriptional phenotypes resemble the ones obtained in the current study where SUB-OX *N. benthamiana* leaves accumulated large amounts of characteristic suberin-type monomers including aromatic components, C20-C24 fatty acids, C20-C24 fatty alcohols, C16-C20 ω-hydroxy acids, and C18:1 ω-hydroxy and diacids. Moreover, SUB transactivated 5' upstream regions of several core suberin biosynthetic genes (*GPAT5*, *ASFT*, *CYP86B1*, *FAR1* and *FAR4*). TEM observations pointed at distinct suberin lamellar structures deposited adjacent to the walls of both epidermal and mesophyll cells of SUB-OX infiltrated leaves. Accordingly, SUB transactivated the promoter of *ABCG6* encoding one of key suberin monomer transporters, and significant increased expression of all known suberin transporters (*ABCG2*, *ABCG6*, *ABCG10*, *ABCG16* and *ABCG20*) were detected in SUB-OX roots. Together, it implies that SUB not only triggers the expression of suberin biosynthesis genes, but also those required to assemble and deposit these unique structures at their pertinent subcellular sites. While it is outstanding that overexpression of SUB alone activated the entire suberin pathway, it is likely that it cooperates with other transcription factors from different families to execute the necessary steps essential for establishing complete suberin lamellae. The set of genes possibly operate with and/or downstream of SUB conceivably include MYB53, MYB92 and MYB93 forming a related phylogenetic cluster with SUB, MYB107 and MYB9. Others might include NAC46 recently shown to promote suberin synthesis in Arabidopsis roots (Mahmood et al., 2019), as well as WRKY56, NAC38, and NAC58, exhibiting substantial upregulation in SUB-OX roots, and were previously suggested to be part of a gene expression signature for suberin biosynthesis (Lashbrooke et al., 2016). An additional layer of regulation might occur through hormonal signaling cascades. In potato tuber for example, ABA upregulates 18:1 ω-hydroxyacid and α,ω-diacid aliphatic suberin biosynthesis (Woolfson et al., 2018), while the endodermal suberin lamellae of Arabidopsis roots are highly plastic in response to ABA and ethylene (Barberon et al., 2016). In accord with these studies, genes involved in ABA and ethylene signaling cascades displayed differential expression in *sub* and SUB-OX roots,

suggesting that the changes detected in suberin pathway in these roots might be mediated via the activity of these two hormones.

Our data raise an important question regarding the spatial and temporal nature of SPPD and SPAD deposition patterns. The higher suberin loads produced by both SUB-OX *N. benthamiana* leaves and Arabidopsis roots were accompanied by elevated ferulic acid levels and the accumulation of phenylpropanoid-associated transcripts. Here, we provide strong evidences that SUB regulates the aliphatic pathway of suberin and most likely the phenolic pathway as well, since the expression of phenylpropanoid-associated genes was highly induced in both *N. benthamiana* and Arabidopsis expressing SUB-OX. In the case of potato, the StWRKY1 was shown to activate promoter regions of the phenylpropanoid genes *4CL* and *THT* thereby affecting the deposition of hydroxycinnamic acid amides (Yogendra et al., 2015). Yet, it was not directly specified with the phenolic pathway of suberin. Additional experiments analyzing the ability of SUB to transactivate phenylpropanoid-associated genes would shed light on its possible regulation of SPPD.

SUBERMAN is a novel regulator of endodermis suberization during Arabidopsis root development

The capacity of root endodermis to function as a successful barrier is achieved by the deposition of lignified Casparian strips and suberin lamellae in its cell walls during its development. It is therefore surprising that no transcription factor was reported to regulate developmental endodermis suberization whereas the regulatory networks involved in Casparian strip formation have been comprehensively elucidated (Roppolo et al., 2011; Kamiya et al., 2015; Liberman et al., 2015; Di Laurenzio et al., 1996; Helariutta et al., 2000; Heidstra et al., 2004; Sozzani et al., 2010; Cui et al., 2007). To date, the promoter of the suberin regulator *AtMYB41* was found to be active in the endodermis, yet only under abiotic stresses and not under normal conditions (Kosma et al., 2014), and therefore cannot be associated with developmental processes. Interestingly, the promoters of *AtMYB107* and *AtMYB9* homologs shown previously to regulate suberin metabolism in the seed coat (Lashbrooke et al., 2016), are also not expressed in roots under normal conditions

(Supplemental Figure 10). Here, we reveal SUB as the first regulator coordinating suberization of root endodermis cell wall during differentiation. The endodermis-specific expression of *SUB* coincided with expression patterns of well-characterized suberin biosynthetic genes as *GPAT5*, *CYP86A1* and *CYP86B1*. *SUB* expression was not detected in early-differentiated endodermal cells that do not produce lamellar suberin, but rather in patchy and continuous suberization root zones. In our assays we used FY that stains only lamellar suberin, and therefore we cannot rule out the presence of diffused non-lamellar suberin in early-differentiated endodermal cells. Indeed, previous anatomical and chemical assays analyzing suberin patterns in soybean roots demonstrated the abundance of aliphatic suberin in state I endodermal cells that contain Casparian strips but no lamellar suberin (Thomas et al., 2007; Ranathunge et al., 2008).

Staining assays and polyester profiling clearly indicated that *sub* roots accumulated lower levels of most typical suberin-type components. In contrast, boosted synthesis of suberin was detected in SUB-OX roots. Various microscopical approaches indicated that the higher degree of suberization in SUB-OX roots could not be attributed only to enhanced accumulation of suberin in the endodermis, but also due to ectopic suberization in the root cortex with some degree of suberization in epidermal cells as well. Moreover, some portion of endodermal cells located in early-differentiated root zones that naturally do not produce suberin, displayed suberized patches. Partial explanation for the unusual existence of suberin in these root regions might be that SUB was capable of inducing ectopic expression of *GPAT5* in all root cell layers beside the endodermis, as well as elevating the expression of *CYP86A1* and *CYP86B1* within the endodermis.

Ectopic suberization was previously reported in mutants that possess defective Casparian strips such as *esb1*, *casp1casp3* and *myb36*, suggesting a cross-talk between formation of lignin and the deposition of suberin lamellae (Kamiya et al., 2015; Hosmani et al., 2013). It was assumed that over-suberization in these roots is part of a compensative response to maintain barrier identity when Casparian strip functionality is limited. Our findings raise an important question whether Casparian strip formation can overcome faulty or ectopic deposition of suberin lamellae such as in *sub* and SUB-OX roots, respectively.

Analyzing Casparian strip formation along the root axis of WT, *sub* and SUB-OX revealed no changes between them, even in root zones where dramatic structural modifications were detected in suberin lamellae. Furthermore, mining our root transcriptome datasets strengthened this notion as *sub* and SUB-OX roots displayed similar expression level of key genes involved in Casparian strip formation and positioning as in WT roots (Supplemental Figure 6). Taken together, these results imply that SUB operates in the frame of endodermis suberization, and when changes in suberin lamellae composition and structure occur due to altered *SUB* expression, it does not affect Casparian strips. The findings here corroborate previous discoveries demarcating endodermis Casparian strip establishment and function from those of the suberin lamellae (Naseer et al., 2012; Barberon et al., 2016; Kamiya et al., 2015; Hosmani et al., 2013; Pfister et al., 2014).

Unlike the metabolism of Casparian strips, many genes involved in the biosynthetic pathways of root cuticular lipids were highly responsive in SUB-OX roots suggesting an interaction between the regulation of the two pathways. Intriguingly, most of these genes did not exhibit any altered expression in the *sub* mutant root. This is reasonable as increased flux of acyl-lipids might fuel not only the enhanced synthesis of suberin but the biosynthetic pathways of cuticular lipids as well, in agreement with a previous report suggesting a common pathway for the biosynthesis of aliphatic suberin and some of the suberin-associated root waxes (Li et al., 2007a). Overall, we show that SUB activity is critical for building the suberin lamellae sealing the walls of the endodermal cells during specific stages of Arabidopsis root development. This mode of regulation is achieved by a developmental and cell-type-specific induction of a battery of genes essential for suberization.

Alterations in endodermis suberin lamellae affect root uptake capacities

Root endodermis suberin lamellae was previously shown to affect water relations and mineral nutrition (Baxter et al., 2009), to take active roles in responses against salt and drought stresses (Krishnamurthy et al., 2009, 2011), and are highly plastic in response to nutritional stress conditions (Barberon et al., 2016). Our data provide additional layer of evidence that endodermis suberization has significant effect on root uptake capacities.

The ectopically deposited suberin in SUB-OX roots likely blocked to some degree their uptake and transport abilities as leaves of these plants exhibited lower levels of various ions and nutrients. For example, lower abundances of Ca, Mn, Fe Co and Sr were detected in SUB-OX leaves, similar to leaves of *myb36* mutant characterized by root ectopic suberization (Kamiya et al., 2015). Ca, Mn, Fe and Sr were also significantly lower in shoots of *esb1* and *casp1casp3* mutants that also possess ectopically suberized roots (Hosmani et al., 2013). We postulate that these ionomic phenotypes are caused by the heavily- and partially-suberized cortical and epidermal cells in SUB-OX roots, respectively, restricting their uptake capabilities. The buildup of PI and FDA tracers in SUB-OX roots support the changes measured in their ionomic profiles. In addition, SUB-OX root transcriptome revealed a large subset of downregulated genes encoding ion and nutrient transporters, for example those involved in uptake of P (*PHT1;1* and *PHT1;4*), K (*HAK5*) and S (*SULTR3;5*). Indeed, all three macronutrients accumulated to lower levels in SUB-OX leaves. Nevertheless, as SUB-OX roots deposited lamellar suberin also in the cortex and epidermis, it is likely that the root apoplastic pathway transporting PI, FDA and ions was affected irrespective of the changes in endodermal suberization that in principal should affect only the transcellular transport.

Unlike the changes observed in ionomic profiles of SUB-OX leaves, *sub* and WT roots and rosette leaves displayed relatively comparable elemental profiles indicating that reduced root endodermis suberin has relatively minor effect on root ion uptake. Our findings display partial similarities with previous studies reporting small ionomic changes in rosette leaves of the two suberin-deficient lines *ELTP::CDEF1* and *CASP1::CDEF1* (Barberon et al., 2016), and of the *sgn3* mutant that has faulty Casparian strips (Pfiser et al., 2014). Nonetheless, *sub* leaves accumulated more P, K and Rb contrasting the above two suberin-deficient lines that actually displayed lower levels of these ions in their leaves. One possible explanation might be that the reduced levels and/or composition of suberin in these systems are dissimilar and thus the changes on root uptake capacities are different.

Conclusions

To summarize, our findings indicate that the SUB transcription factor plays an essential role in regulating the developmental suberization of endodermis in the Arabidopsis root. SUB regulates promoter regions of suberin biosynthetic, transport and regulatory genes to initiate the deposition of suberin lamellae sealing the walls of endodermal cells during their development and differentiation. In the absence of SUB, the barrier function of suberin lamellae is hampered, causing reductions in endodermis suberin contents and gene transcripts. Surprisingly, these had relatively mild effect on root uptake capabilities. When SUB is overexpressed, ectopic deposition of suberin lamellae occur at all root cell layers to various degrees, likely blocking transcellular uptake of some ions and minerals into the endodermis and xylem vessels. The findings obtained here provide an important milestone towards dissecting the molecular mechanisms involved in the performance of the endodermal barrier.

Methods

Plant material and growth conditions

Arabidopsis (Columbia-0) and *N. benthamiana* seeds were stratified at 4 °C for 2-3 days and then sown in a nutritional-rich soil medium in 8 cm x 8 cm x 6 cm (0.4 L) pots. Seedlings were grown in environmentally-controlled growth rooms at 22 °C, 70% humidity and 18/6 hours of light/dark cycles. A *sub* (i.e. *myb39*; SALK_111635) T-DNA insertion line was identified using the SIGnAL T-DNA Express Arabidopsis Gene Mapping Tool (http://signal.salk.edu/cgi-bin/tdnaexpress). This line harbors a T-DNA insertion located in an exon of its coding region (chromosome 4 position 9,882,304) and was genotyped using specific oligonucleotides designed in T-DNA PrimerDesign (http://signal.salk.edu/tdnaprimers.2.html) (see genotyping oligonucleotides in Supplemental Table 4).

Vector construction and plant transformation

Binary vectors were generated using the GoldenBraid cloning system (Sarrion-Perdigones et al., 2013). For making SUB-OX, full-length genomic *SUB* (At4G17785) sequence amplified using the 'Phusion' DNA Polymerase (Finnzyme) kit, cloned into the universal plasmid (pUPD) which was ligated to a pUPD containing the tomato *UBIQUITIN10* (pSlUBQ1) constitutive promoter and transferred into a 3α2 vector, which was further ligated to a 3α1 vector harboring the kanamycin resistance gene and finally to the 3Ω1 transformation plasmid (Sarrion-Perdigones et al., 2013).

For construction of promoter-reporter lines of AtSUB, AtMYB9 (At4G17785) and AtMYB107 (At3G02940), a pUPD vector containing RFP was ligated separately to pUPD vectors harboring the native ~3000 bp 5' upstream regions of these genes, into a 3α2 vector. For subcellular localization of SUB, the C-terminus region of its coding sequence was fused in-frame with an enhanced GFP and subsequently inserted into a 3α2 vector. Both types of reporter vectors were then ligated together with a 3α1 vector harboring the kanamycin resistance gene into 3Ω1.

For making transactivation vectors the native 5' upstream regions (~2500 bp) of Arabidopsis GPAT5 (AT3G11430), ASFT (AT5G41040), CYP86B1 (AT5G23190), ABCG6 (AT5G13580), FAR1 (AT5G22500), FAR4 (AT3G44540), MYB9, MYB41, MYB107, SUB and tomato *GLYCOALKALOID METABOLISM 1* (SlGAME1), were amplified and cloned into pUPD vectors. Each of these pUPDs were then cloned together with two pUPD vectors, the first contains the firefly *luciferase* (Luc) reporter gene (GeneBank: X84847) fused to the CaMV 35S terminator, and the second harbors the renilla *luciferase* (Ren) reporter gene (GeneBank: P05938) fused to the SlUBQ10 promoter and respective terminator. These elements were inserted simultaneously into a 3α1 vector thereby forming individual luciferase transformation vectors where Luc used as the induction reporter and Ren as the normalizing reporter. Transformation vectors, including an empty vector control (a 3Ω1 plasmid without an insert harboring the LACZ gene), were transformed into *Agrobacterium tumefaciens* (GV3101 strain) using a micropulser electroporator (Bio-Rad). Arabidopsis (Columbia-0) plants were transformed with floral dip method and at least 10 independent transgenes per vector were used for further work in subsequent generations.

Transient expression of SUB-OX in *N. benthamiana* leaves

Agroinfiltration experiment was performed as previously described (Sparkes et al., 2006). Leaf discs were harvested 5 days post infiltration and either snap-frizzed for RNA extraction and further gene expression assays, delipidated in 1:1 (v:v) $CHCl_3$/MeOH for a two-weeks at constant agitation and daily replacement of fresh delipidation solution prior to polyester profiling by GC-MS, or immersed in fixation buffer for further TEM examinations.

Transactivation luciferase assay, subcellular localization and promoter-reporter experiments

Transactivation luciferase assay was performed as previously described (McNabb et al., 2005). Bioluminescence of both Luc and Ren was measured by a luminometer (Turner BioSystems), and Luc/Ren ratios were calculated for every treatment as compared to its respective EV. Control assays validating the assay's feasibility were performed by infiltrating *N. benthamiana* leaves with a negative control double-distilled water, a positive control where Luc was fused to the constitutive *pSlUBQ10* promoter, or using the *SlGAME1* promoter. For every treatment, 4 biological replicates were assayed each generated from a pool of leaves from 4 different infiltrated plants. SUB subcellular localization was achieved by co-infiltrating the vector pSlUBQ::AtSUB-eGFP together with a plasmid harboring the nuclear fluorescent reporter p35S::4xNLS-mRFP into 6-week-old *N. benthamiana* leaves. Representative leaf discs were isolated 24 hours post infiltration, and epidermis pavement cells were observed for GFP (488 nm) and RFP (647 nm) fluorescent signals using a Confocal Laser Scanning Microscope (CLSM; Nikon Eclipse A1). To analyze promoter-reporter lines of *AtSUB*, *AtMYB9* and *AtMYB107*, RFP (647 nm) signals were observed by CLSM in various tissues from 8-week-old Arabidopsis pAtSUB::RFP, pAtMYB9::RFP and pAtMYB107::RFP lines.

Staining and penetration assays

Histochemical detection of suberin was achieved by staining 10-day-old roots with a freshly prepared solution of fluorol yellow 088 (0.01% w/v in lactic acid) for 30 min at 70 ºC. Following washing in water, roots were observed for suberin by a CLSM under the GFP filter with or without propidium iodide (PI) counterstaining for cell wall under the RFP filter. Specifically for CLSM analyses of *SUB* spatial expression in pSUB::RFP root cell walls were counterstained with Calcofluor white (0.1% v/v in double distilled water). Quantification of suberization degree in different zones along the root axis of WT, *sub* and SUB-OX were performed as previously described (Barberon et al., 2016). Casparian strip autofluorescence and quantification of endodermal cells displaying Casparian strip blockage to PI were performed by a CLSM under the GFP filter as previously described (Naseer et al., 2012). For *β*-glucuronidase staining, 10-day-old plants roots were suspended and vacuum-infiltrated for 30 min in a *β*-glucuronidase staining solution (0.1 M NaH_2PO_4 at pH 7.0, 10 mM Na_2-ethylenediaminetetraacetic acid, 0.5 mM K-ferricyanide, 0.5 mM K-ferrocyanide, 1.0 mM X-glucuronide prepared freshly in DMSO, 0.1% Triton X-100). Root samples were then incubated at 37 °C for 24 hours until staining was visible. Stained tissues were fixed in a mixture of ethanol:acetic acid:formaldehyde (50:5:3.7, v/v) for 10 min at 65 °C and de-stained in 80% (v/v) ethanol until removal of chlorophyll. Images of whole roots and closer examinations of endodermis staining patterns were obtained by a light microscope (Olympus CLSM500). For penetration assays**,** roots were monitored for their uptake capacities of two fluorescent apoplastic tracers, propidium iodide (PI) and fluorescein diacetate (FDA). Ten-day-old roots were incubated in the dark for 10 min in a freshly-prepared 15 µM PI staining solution (10 mg w/v in double distilled water) and then immediately observed by a CLSM under a 561 nm filter. A time-lapse penetration assay was performed by a 30 sec incubation of 10-day-old roots in the dark in a freshly-prepared FDA staining solution (5 µg w/v in double distilled water). Stained roots were then counterstained with PI and immediately observed by a CLSM under a GFP and RFP filters. Images of both PI and FDA signals were captured on a time-lapse manner every 30 sec until 15 min since the beginning of capturing.

Transmission electron microscopy

Ten-day-old roots grown on a nutritional-rich MS-agar medium were gently fixed in electron microscopy-grade 4% PFA (v/v) and 2% GA (v/v) in cacodylate 0.1 M buffer. Following fixation, samples were stained with Osmium (OsO_4) and uranyl acetate, dehydrated in a graded ethanol series and infiltrated with 100% Epon, using an automated robot. Ultrathin sections were performed using a Leica 2000 microtome and mounted on TEM grids. Sections were observed with a Technai T12 TEM apparatus.

Elemental profiling using Inductively Coupled Plasma-Mass Spectrometry (ICP-MS)

Elemental profiling was performed on 3-week-old plants grown on a nutrient-rich soil medium mixed with vermiculite. Roots and rosette leaves were isolated and allowed to fully dry in an oven at 60 ºC for 48 hours. Samples were digested with 900 µL of 70% HNO_3 (≥99.999% trace metals basis, Sigma-Aldrich) and diluted to a final volume of 4 ml with ultrapure water (18.2 MΩcm). The following elements: Li, B, Na, Mg, P, S, K, Ca, Mn, Fe, Co, Ni, Cu, Zn, As, Se, Rb, Sr, Mo and Cd, were measured using an Inductively Coupled Plasma-Mass Spectrometry (ICP-MS) coupled to an autosampler injecting apparatus (Agilent Technologies 7700 Series, Santa Clara, USA). ICP-MS system was calibrated with 0, 1, 2, 5, 10, 50, 100, 500, 1000, 1500, 2000 and 2500 ppb certified ICP-MS calibration standard solutions (IV-STOCK-21, Inorganic Ventures, USA) prepared in 1% HNO_3 (v/v; ≥99.999% trace metals basis, Sigma-Aldrich). Internal standard solution containing 1000 ppb of Gadolinium (certified Gadolinium stock solution CGGD1, Inorganic Ventures, USA) was injected throughout the duration of measurements for normalization and technical error correction purposes. Determination of elements was done using an Octapole Reaction cell (ORS^3) for minimization of spectral interferences and averaged numerical value for each element was calculated from triplicate measurements using the MassHunter v4.1 Work Station Software for 7700 ICP-MS (Agilent Technologies, Inc. 2015). For part of the samples, a further 10-fold dilution was performed to adjust the final concentrations within the range of calibration curves. Final elements' concentrations were calculated following the normalization to Gadolinium internal standard and dry weights.

Gene expression analyses

Total RNA was extracted from various tissues using the Spectrum Total RNA Kit (Sigma-Aldrich) according to manufacturer protocols. RNA concentrations and purity levels were quantified using a standard nanodrop and then treated with DNase (DNase I; Sigma-Aldrich). cDNA was synthesized using a High Capacity cDNA Reverse Transcription Kit (Applied Biosystems). For gene expression analyses, quantitative real-time q(RT)-PCR was employed using specific forward and reverse oligonucleotides designed according to the tools embedded in the NCBI Primer BLAST platform (https://www.ncbi.nlm.nih.gov/tools/primer-blasta). Oligonucleotides were calibrated for specificity by analyzing their melting curves and for efficiency using calibration curves (R^2 > 0.9 and 90-110% efficiency). q(RT)-PCR reactions were performed on a StepOnePlus Real-Time PCR system (Applied Biosystems) using the FAST SYBR Green Master Mix (Applied Biosystems). Gene expression was normalized either to the Arabidopsis ubiquitous gene *PROTEIN PHOSPHATASE 2* (*PP2A*) or the *N. benthamiana* ubiquitous genes *PROTEIN PHOSPHATASE 2* (*PP2A*) and *F-BOX*, according to the respective experiment. Assays were performed on 3 biological replicates each per sample. Oligonucleotides used for q(RT)-PCR assays appear in Supplemental Table 4. For transcriptome analysis, high quality RNA was used for preparation of strand specific TranSeq libraries for Illumina high-throughput sequencing as recently described (Tzfadia et al., 2018). Libraries were examined for purity and integrity before analysis using the Illumina Hi-Seq 2000 under default parameters generating 50 bp single end reads. Reads were mapped to the recent published genome of Arabidopsis (TAIR10; The Arabidopsis Information Resource; www.arabidopsis.org) generating normalized RPKM values for each gene.

Profiling of suberin monomers

N. benthamiana leaf discs agroinfiltrated with an EV control or SUB-OX, and 10-day-old roots grown on a nutritional-rich MS-agar medium, were analyzed for polyester compositions by a Gas Chromatography-Mass Spectrometry (GC-MS) as recently described (Cohen et al.,

2019). Integrated peaks of mass fragments were normalized for sample dry weight as well as the respective C_{32}-alkane internal standard signal for each sample individually.

Statistical analyses

Bar graphs were compiled using the GraphPad Prism 5.01 scientific software (http://www.graphpad.com/) and significance was calculated according to two-tailed *t*-test of *P* value < 0.05 or one-way ANOVA of *P* value < 0.05 depending on specific experiment. In the case of ICP-MP elemental profiling assay the two-tailed *t*-test of *P* value < 0.05 was employed following multiple comparison correction according the Holm-Sidak method. Principal Component Analysis (PCA) of TranSeq data was performed using MetaboAnalyst 4.0 (http://metaboanalyst.ca/) (Chong et al., 2018) following data $\log_{10}$-transformation and pareto scaling (mean centered and divided by the square root of standard deviation of each variable) manipulations. Venn diagram of TranSeq data were generated using Venny (http://bioinfogp.cnb.csic.es/tools/venny/) and Gene Ontology (GO) analysis with AgriGO (http://systemsbiology.cau.edu.cn/agriGOv2/) (Tian et al., 2017).

DATA AVAILABILITY STATEMENT

The authors confirm that all experimental data are available and accessible via the main text and/or the supplemental data.

ACKNOWLEDGMENTS

We wish to acknowledge Eyal Shimoni and Guy Shmul for assistance in TEM and ICP-MS experiments, respectively, and Georg Jander for critical reading of the manuscript. We are grateful to the Adelis Foundation, the Leona M. and Harry B. Helmsley Charitable Trust, the Jeanne and Joseph Nissim Foundation for Life Sciences, and especially the Tom and Sondra Rykoff Family Foundation Research for supporting the A.A. lab activity. A.A. is the incumbent of the Peter J. Cohn Professorial Chair.

AUTHOR CONTRIBUTIONS

The scientific concept and the experimental design were developed by H.C. and A.A. H.C. and V.F. performed all experiments. H.C., V.F., C.W., S.W. and A.A. analyzed the data. H.C. and A.A. wrote the manuscript. All contributing authors approved the manuscript and agreed to be accountable for all aspects of the work.

CONFLICT OF INTEREST

The authors declare that they have no conflicts of interest.

REFERENCES

Andersen TG, Barberon M, Geldner N. (2015) Suberization – the second life of an endodermal cell. *Curr. Opin. Plant. Biol.* **28:** 9-15.

Barberon M, Vermeer JE, De Bellis D, Wang P, Naseer S, Anderson TG, Humbel BM, Nawrath C, Takano J, Salt DE, Geldner N. (2016) Adaptation of root function by nutrient-induced plasticity of endodermal differentiation. *Cell.* **164**: 447-459.

Barberon M. (2017) The endodermis as a checkpoint for nutrients. *New. Phytol.* **213**: 1604-1610.

Baxter I, Hosmani PS, Rus A, Lahner B, Borevitz JO, Muthukumar B, Mickelbart MV, Schreiber L, Franke RB, Salt DE. (2009). Root suberin forms an extracellular barrier that affects water relations and mineral nutrition in Arabidopsis. *PLoS. Genet.* **5**: e1000492.

Beisson F, Li Y, Bonaventure G, Pollard M, Ohlrogge JB. (2007) The acyltransferase GPAT5 is required for the synthesis of suberin in seed coat and root of Arabidopsis. *Plant. Cell.* **19:** 351-368.

Beisson F, Li-Beisson Y, Pollard M. (2012) Solving the puzzles of cutin and suberin polymer biosynthesis. *Curr. Opin. Plant. Biol.* **15:** 329-337.

Bernard A, Domergue F, Pascal S, Jetter R, Renne C, Faure JD, Haslam RP, Napier JA, Lessire R, Joubes J. (2012) Reconstruction of plant alkaline biosynthesis in yeast demonstrates that Arabidopsis ECERIFERUM1 and ECERIFERUM3 are core components of a very-long-chain alkane synthesis complex. *Plant. Cell.* **24:** 3106-3118.

Bernards MA. (2002) Demystifying suberin. *Can. J. Bot.* **80:** 227-240.

Bernards MA, Lopez ML, Zajicek J, Lewis NG. (1995) Hydroxycinnamic acid-derived polymers constitute the polyaromatic domain of suberin. *J. Biol. Chem.* **270:** 7382-7386.

Bernards MA, Razem FA. (2001) The poly(phenolic) domain of potato suberin: a non-lignin cell wall biopolymer. *Phytochemistry.* **57:** 1115-1122.

Capote T, Barbosa P, Usie A, Ramos AM, Inacio V, Ordas R, Goncalves S, Morias-Cecilio L. (2018) ChIP-Seq reveals that QsMYB1 directly targets genes involved in lignin and suberin biosynthesis pathways in cork oak (*Quercus suber*). *BMC. Plant. Biol.* **18:** s12870.

Chong J, Saufan O, Li C, Caraus I, Li S, Bourque G, Wishart DS, Xia J. (2018) MetaboAnalyst4.0: towards more transparent and integrative metabolomics analysis. *Nucl. Acids. Res.* **46:** 486-494.

Cohen H, Dong Y, Szymanski JJ, Lashbrooke JG, Meir S, Almekias-Siegel E, Zeisler-Diehl VV, Schreiber L, Aharoni A. (2019) A multilevel study of melon fruit reticulation provides insight into skin lign-suberization hallmarks. *Plant. Physiol.* **179:** 1486-1501.

Cohen H, Szymanski JJ, Aharoni A. (2017) Assimilation of 'omics' strategies to study the cuticle layer and suberin lamellae in plants. *J. Exp. Bot.* **68:** 5389-5400.

Compagnon V, Diehl P, Benveniste I, Meyer D, Schaller H, Schreiber L, Franke R, Pinot F. (2009) CYP86B1 is required for very long chain omega-hydroxyacid and alpha, omega-dicarboxylic acid synthesis in root and seed suberin polyester. *Plant. Physiol.* **150:** 1831-1843.

Cui H, Levesque MP, Vernoux T, Jung JW, Paquette AJ, Gallagher KL, Wang JY, Blilou I, Scheres B, Benfey PN. (2007) An evolutionary conserved mechanism delimiting SHR movement defines a single layer of endodermis in plants. *Science.* **316:** 421-425.

Di Laurenzio L, Wysocka-Diller J, Malamy JE, Pysh L, Helariutta Y, Freshour G, Feldman KA, Benfey PN. (1996) The *SCARECROW* gene regulates an asymmetric cell division that is essential for generating the radian organization of the Arabidopsis root. *Cell.* **86:** 423-433.

Domergue F, Vishwanath SJ, Joubès J, Ono J, Lee JA, Bourdon M, Alhattab R, Lowe C, Pascal S, Lessire R, Rowland O. (2010) Three Arabidopsis fatty acyl-coenzyme A reductases, FAR1, FAR4, and FAR5, generate primary fatty alcohols associated with suberin deposition. *Plant. Physiol.* **153:** 1539-1554.

Dubos C, Stracke R, Grotewold E, Weisshaar B, Martin C, Lepiniec L. (2010) MYB transcription factors in Arabidopsis. *Trends. Plant. Sci.* **15:** 573-581.

Franke R, Briesen I, Wojciechowski T, Faust A, Yephremov A, Nawrath C, Schreiber L. (2005) Apoplastic polyesters in Arabidopsis surface tissues: a typical suberin and a particular cutin. *Phytochemistry.* **66:** 2643-2658.

Franke R, Höfer R, Briesen I, Emsermann M, Efremova N, Yephremov A, Schreiber L. (2009) The DAISY gene from Arabidopsis encodes a fatty acid elongase condensing enzyme involved in the biosynthesis of aliphatic suberin in roots and the chalaza-micropyle region of seeds. *Plant. J.* **57:** 80-95.

Franke R, Schreiber L. (2007) Suberin - a biopolyester forming apoplastic barriers. *Curr. Opin. Plant. Biol.* **10:** 252-259.

Gou JY, Yu XH, Liu CJ. (2009) A hydroxycinnamoyltransferase responsible for synthesizing suberin aromatics in Arabidopsis. *Proc. Natl. Acad. Sci. USA.* **106:** 18855-18860.

Gou M, Hou G, Yang H, Zhang X, Cai Y, Kai G, Liu CJ. (2017) The MYB107 transcription factor positively regulates suberin biosynthesis. *Plant. Physiol.* **173:** 1045-1058.

Heidstra R, Welch D, Scheres B. (2004) Mosaic analyses using marked activation and deletion clones dissect Arabidopsis SCARECROW action in asymmetric cell division. *Genes. Dev.* **18:** 1964-1969.

Helariutta Y, Fukaki H, Wysocka-Diller J, Nakajima K, Jung J, Sena G, Hauser MT, Benfey PN. (2000) The *SHORT-ROOT* gene controls radial patterning pf the *Arabidopsis* root through radial signaling. *Cell.* **101:** 555-567.

Hofer R, Briesen I, Beck M, Pinot F, Schreiber L, Franke R. (2008) The Arabidopsis cytochrome P450 CYP86A1 encodes a fatty acid omega-hydroxylase involved in suberin monomer biosynthesis. *J. Exp. Bot.* **59:** 2347-2360.

Hosmani PS, Kamiya T, Danku J, Naseer S, Geldner N, Guerinot ML, Salt DE. (2013) Dirigent domain-containing protein is part of the machinery required for formation of the lignin-based Casparian strip in the root. *Proc. Natl. Acad. Sci. USA.* **110:** 14498-14503.

Kamiya T, Borghi M, Wang P, Danku JMC, Kalmbach L, Hosmani PS, Naseer S, Fujiwara T, Geldner N, Salt DE. (2015) The MYB36 transcription factor orchestrates Casparian strip formation. *Proc. Natl. Acad. Sci. USA.* **112:** 10533-10538.

Kosma DK, Murmu J, Razeq FM, Santos P, Bourgault R, Molina I, Rowland O. (2014) AtMYB41 activates ectopic suberin biosynthesis and assembly in multiple plant species and cell types. *Plant. J.* **80:** 216-229.

Krishnamurthy P, Ranathunge K, Franke R, Prakash HS, Schreiber L, Mathew MK. (2009). The role of root apoplastic transport barriers in salt tolerance of rice (*Oryza sativa* L.). *Planta.* **230**: 119-134.

Krishnamurthy P, Ranathunge K, Nayak S, Schreiber L, Mathew MK. (2011). Root apoplastic barriers block Na+ transport to shoots in rice (*Oryza sativa* L.). *J. Exp. Bot.* **62**: 4215-4228.

Lashbrooke J, Cohen H, Levy-Samoha D, Tzfadia O, Panizel I, Zeisler V, Massalha H, Stern A, Trianotti L, Schreiber L, Costa F, Aharoni A. (2016) MYB107 and MYB9 homologs regulate suberin deposition in angiosperms. *Plant. Cell.* **28:** 2097-2116.

Lee SB, Jung SJ, Go YS, Kim HU, Kim JK, Cho HJ, Park OK, Suh MC. (2009) Two Arabidopsis 3-ketoacyl CoA synthase genes, KCS20 and KCS2/DAISY, are functionally redundant in cuticular wax and root suberin biosynthesis, but differentially controlled by osmotic stress. *Plant. J.* **60:** 462-475.

Lee SB, Suh MC. (2018) Disruption of glycosylphosphatidylinositol-anchored lipid transfer protein 15 affects seed coat permeability in Arabidopsis. *Plant. J.* **96:** 1026-1217.

Legay S, Guerreriero G, Andre C, Guignard C, Cocco E, Charton S, Boutry M, Rowland O, Hausman JF. (2016) MdMYB93 is a regulator of suberin deposition in russeted apple fruit skins. *New. Phytol.* **212:** 977-991.

Levesque MP, Vernoux T, Busch W, Cui H, Wang JY, Blilou I, Hassan H, Nakajima K, Matsumoto N, Lohmann JU, Scheres B, Benfey PN. (2006) Whole-genome analysis of the SHORT-ROOT developmental pathway in Arabidopsis. *PLoS. Biol.* **4:** e143.

Li Y, Beisson F, Ohlrogge J, Pollard M. (2007a) Monoacylglycerols are components of root waxes and can be produced in the aerial cuticle by ectopic expression of a suberin-associated acyltransferase. *Plant. Physiol.* **144**: 1267-1277.

Li Y, Beisson F, Koo AJ, Molina I, Pollard M, Ohlrogge J. (2007b) Identification of acyltransferases required for cutin biosynthesis and production of cutin with suberin-like monomers. *Proc. Natl. Acad. Sci. USA.* **104:** 18339-18344.

Liberman LM, Sparks EE, Moreno-Risueno MA, Petricka JJ, Benfey PN. (2015) MYB36 regulates the transition from proliferation to differentiation in the Arabidopsis root. *Proc. Natl. Acad. Sci. USA.* **112:** 12099-12104.

Lux A, Morita S, Abe J, Ito K. (2005) An improved method for clearing and staining free-hand sections and whole-mount samples. *Ann. Bot.* **96:** 989-996.

Mahmood K, Zeisler-Diehl VV, Schreiber L, Bi YM, Rothstein SJ, Ranathunge K. (2019) Overexpression of ANAC046 promotes suberin biosynthesis in root of *Arabidopsis thaliana*. *Int. J. Mol.* **20:** 6017.

McNabb DS, Reed R, Marciniak RA. (2005) Dual luciferase assay system for rapid assessment of gene expression in *Saccharomyces cerevisiae*. *Eukaryotic. Cell.* **4:** 1539-1549.

Molina I, Li-Beisson Y, Beisson F, Ohlrogge JB, Pollard M. (2009) Identification of an Arabidopsis feruloyl-coenzyme A transferase required for suberin synthesis. *Plant. Physiol.* **151:** 1317-1328.

Naseer S, Lee Y, Lapierre C, Franke R, Nawrath C, Geldner N. (2012) Casparian strip diffusion barrier in *Arabidopsis* is made of lignin polymer without suberin. *Proc. Natl. Acad. Sci. USA.* **109:** 10101-10106.

Panikashvili D, Savaldi-Goldstein S, Mendel T, Yifhar T, Franke RB, Hofer R, Schreiber L, Chory J, Aharoni A. (2007) The Arabidopsis DESPERDAO/AtWBC11 transporter is required for cutin and wax secretion. *Plant. Physiol.* **145:** 1345-1360.

Pfister A, Barberon M, Alassimone J, Kalmbach L, Lee Y, Vermeer JE, Yamazaki M, Li G, Maurel C, Takano J, Kamiya T, Salt DE, Roppolo D, Geldner N. (2014) A receptor-like kinase mutant with absent endodermal diffusion barrier displays selective nutrient homeostasis defects. *eLife.* **3:** e03115.

Ranathunge K, Thomas RH, Fang X, Peterson CA, Gijzen M, Bernards MA. (2008) Soybean root suberin and partial resistance to root rot caused by *Phytophtora sojae*. *Phytopathology.* **98:** 1179-1189.

Roppolo D, De Rybel B, Tendon VD, Pfister A, Alassimone J, Vermeer JEM, Yamazaki M, Stierhof YD, Beeckman T, Geldner N. (2011) A novel protein family mediates Casparian strip formation in the endodermis. *Nature.* **473:** 380-383.

Sarrion-Perdigones A, Vazquez-Vilar M, Palaci J, Castelijns B, Forment J, Ziarsolo P, Blanca J, Granell A, Orzaez D. (2013) GoldenBraid 2.0: a comprehensive DNA assembly framework for plant synthetic biology. *Plant. Physiol.* **162:** 1618-1631.

Schreiber L, Hartmann K, Skrabs M, Zeier J. (1999) Apoplastic barriers in roots: chemical composition of endodermal and hypodermal cell walls. *J. Exp. Bot.* **50:** 1267-1280.

Schreiber L. (2010) Transport barriers made of cutin, suberin and associated waxes. *Trends. Plant. Sci.* **15:** 546-553.

Sozzani R, Cui H, Moreno-Risueno MA, Busch W, Van Norman JM, Vernoux T, Brady SM, Dewitte W, Murry JA, Benfey PN. (2010) Spatiotemporal regulation of cell-cycle gene by SHORTROOT links patterning and growth. *Nature.* **466:** 128-132.

Sparkes IA, Runions J, Kearns A, Hawes C. (2006) Rapid, transient expression of fluorescent fusion proteins in tobacco plants and generation of stably transformed plants. *Nat. Protoc.* **1:** 2019-2025.

Thomas R, Fang X, Ranathunge K, Anderson TR, Peterson CA, Bernards MA. (2007) Soybean root suberin: anatomical distribution, chemical composition, and relationship to partial resistance to *Phytophtora sojae*. *Plant. Physiol.* **144:** 299-311.

Tian T, Liu Y, Yan HY, You Q, Yi X, Du Z, Xu WY. (2017) agriGO v2.0: a GO analysis toolkit for the agricultural community, 2017 update. *Nucl. Acids. Res.* **45:** 122-129.

Tzfadia O, Bocobza S, Defroot J, Almekias-Siegel E, Panda S, Levy M, Storme V, Rombauts S, Jaitin DA, Keren-Shaul H, Van de Peer Y, Aharoni A. (2018) The 'TranSeq' 3' end sequencing method for high throughput transcriptomics and gene space refinement in plant genomes. *Plant. J.* **96:** 223-232.

Ursache R, Anderson TG, Marhavy P, Geldner N. (2018) A protocol for combining fluorescent proteins with histological stains for diverse cell wall components. *Plant. J.* **93:** 399-412.

Verdaguer R, Soler M, Serra O, Garotte A, Fernandez S, Company-Arumi D, Antico E, Molinas M, Figueras M. (2016) Silencing of the potato StNAC103 gene enhances the accumulation of suberin polyester and associated wax in tuber skin. *J. Exp. Bot.* **67:** 5415-5427.

Vishwanath SJ, Kosma DK, Pulsifer IP, Scandola S, Pascal S, Joubès J, Dittrich-Domergue F, Lessire R, Rowland O, Domergue F. (2013) Suberin-associated fatty

alcohols in Arabidopsis: distributions in roots and contributions to seed coat barrier properties. *Plant. Physiol.* **163:** 1118-1132.

Woolfson KN, Haggitt ML, Zhang Y, Kachura A, Bjelica A, Rincon MAR, Kaberi KM, Bernards MA. (2008) Differential induction of polar and non-polar metabolism during wound-induced suberization in potato (*Solanum tuberosum* L.) tubers. *Plant. J.* **93:** 931-942.

Yadav V, Molina I, Ranathunge K, Castillo IQ, Rothstein SJ, Reed JW. (2014) ABCG transporters are required for suberin and pollen wall extracellular barriers in Arabidopsis. *Plant. Cell.* **26:** 3569-3588.

Yogendra KN, Kumar A, Sarkar K, Li Y, Pushpa D, Mosa KA, Duggavathi R, Kushalappa AC. (2015) Transcription factor StWRKY1 regulates phenylpropanoid metabolites conferring late blight resistance in potato. *J. Exp. Bot.* **66:** 7377-7389.

FIGURE LEGENDS

Figure 1. Transient expression of *SUBERMAN* induces the accumulation of suberin and the deposition of suberin-like lamellae in *N. benthamiana* leaves.

(A) Transmission Electron Microscopy (TEM) images showing cell wall ultrastructure of epidermal and mesophyll cells of *N. benthamiana* leaf sections agroinfiltrated with an empty vector (EV) control or the SUB-OX vector. Bars in square micrographs represent 200 nm while those in rectangle micrographs represent 20 nm. PCW, primary cell wall; SL, suberin lamellae; C, cuticle layer. Mitochondria, chloroplasts and Golgi apparatus are marked.

(B) Leaf polyester content in *N. benthamiana* leaf sections agroinfiltrated with an EV or SUB-OX, measured by Gas Chromatography-Mass Spectrometry (GC-MS). The *y*-axis represents relative peak areas following normalization to a C_{32}-alkane internal standard. ω-OH, ω-hydroxy fatty acids; DCAs, dicarboxylic fatty acids; di-OH C16:0, 10(9),16-dihydroxy fatty acid.

(C) Expression of genes involved in the biosynthesis of suberin, cuticle, and phenylpropanoid and lignin, in *N. benthamiana* leaf sections agroinfiltrated with an EV or SUB-OX, measured by quantitative Real Time q(RT)-PCR. The *y*-axis represents relative gene expression following the normalization to endogenous constitutive *N. benthamiana* genes *PROTEIN PHOSPHATASE 2* (*PP2A*) and *F-BOX*.

Data in [B] and [C] represent mean ± s.e. of three biological replicates each generated from a pool of four infiltrated leaves and data points denote individual biological replicates. Orange asterisks indicate statistically significant differences as compared to EV determined by two-tailed *t*-test of P value < 0.05.

Figure 2. *SUB* is expressed in endodermal cells displaying patchy and continuous suberization.

(A) Confocal Laser Scanning Microscopy (CLSM) images showing endodermis-specific expression of RFP driven by the native 5' upstream region of the *SUB* gene (pAtSUB::RFP) in the Arabidopsis root. Root cell layers are highlighted by Calcofluor white (cyan). Note the

RFP signals (647 nm) detected in patchy and continuous suberized root zones but not in the non-suberized zone. Dashed lines in longitudinal *Z* projections represent areas of cross section views. Bars represent 50 μm.

(B) CLSM images showing nuclear localization of SUB in *N. benthamiana* leaves co-infiltrated with pSIUBQ10::AtSUB-eGFP and p35S::4xNLS-RFP vectors. Images show GFP (SUB), RFP (nucleus marker) and Cy5 (chlorophyll autofluorescence) signals. Overlay image encapsulates all three signals with bright filed. Enlarged square in the overlay image shows co-localization of GFP (SUB protein) and nuclear RFP. Bars represent 20 μm.

Figure 3. Roots with altered *SUB* expression display changes in suberin profiles.

(A) CLSM images displaying the accumulation patterns of suberin along the root axis of WT, *sub* and SUB-OX plants (*Z* projections). Root cell layers are highlighted by propidium iodide (PI; red) while suberin (yellow) was histochemically detected by FY staining. Bars represent 50 μm.

(B) Quantification of suberization degree in different zones along the root axis of WT, *sub* and SUB-OX, presented as the percentage (%) of endodermal cells. Data in bars represent means ± s.e. of ten biological replicates with small letters indicate statistically significant differences determined by one-way ANOVA of P value < 0.05.

(C) TEM images showing cell wall ultrastructure and suberin lamellae in epidermis, cortex and endodermis of WT, *sub* and SUB-OX roots. Images were obtained from similar regions in the continuous suberized zones from the three root genotypes. Arrows point to suberin lamellae (SL). Bars represent 40 nm.

(D) Root suberin profile measured by GC-MS. The *y*-axis represents relative peak areas following normalization to a C_{32}-alkane internal standard. Data in bars represent means ± s.e. of three biological replicates denoted by data points. Orange asterisks indicate statistically significant differences as compared to WT determined by two-tailed *t*-test of P value < 0.05. ω-OH, ω-hydroxy fatty acids; DCAs, dicarboxylic fatty acids.

Figure 4. SUB transactivates upstream regions of genes acting in suberin biosynthesis, transport and pathway regulation.

(A) CLSM images displaying the expression of GFP driven by the native 5' upstream regions of *GPAT5*, *CYP86A1* or *CYP86B1* genes in continuous suberized root zones of pGPAT5::NLS-GFP-GUS, pCYP86A1::NLS-GFP-GUS and pCYP86B1::NLS-GFP-GUS reporter lines non-transformed or ones transformed with SUB-OX. Root cell layers are highlighted by PI staining (red). Bars represent 50 µm.

(B) Diagrams of effector and reporter vectors used for the transactivation luciferase assay depicted in [C]. Full names of all genes and controls used in this assay are listed in Supplemental Figure 7.

(C) Transactivation luciferase assay measuring the capacity of the SUB transcription factor to induce upstream regions in the promoter regions of suberin genes. The *y*-axis represents fold changes of *luciferase* (Luc) to *renilla* (Ren) rations between SUB-OX as compared to EV. Data in bars represent mean ± s.e. of four biological replicates each generated from a pool of four infiltrated leaves and data points denote individual biological replicates. Orange asterisks indicate statistically significant differences as compared to EV determined by two-tailed *t*-test of P value < 0.05.

Figure 5. Alterations in endodermis suberin lamellae affect root uptake capacities.

(A) CLSM images displaying PI penetration across cell layers of WT, *sub* and SUB-OX roots. Images were taken from similar parts of continuous suberized zones of all three genotypes 5 minutes following PI application. Bars represent 75 µm. ep, epidermis; c, cortex; en, endodermis.

(B) CLSM images showing fluorescein diacetate (FDA) penetration across cell layers of WT, *sub* and SUB-OX roots. Representative images were taken from similar parts of continuous suberized zones of all three genotypes 2 to 12 minutes following FDA application in 2 minutes intervals. Bars represent 50 µm. ep, epidermis; c, cortex; en, endodermis.

(C) Elemental composition analysis performed in roots and rosette leaves harvested from WT, *sub* and SUB-OX 3-week-old plants. Elements were determined by Inductively Coupled

Plasma-Mass Spectrometry (ICP-MS) analysis. The heatmap represents the fold-change of each element per tissue compared to the corresponding WT tissue. Red asterisks indicate statistically significant differences as compared to WT determined by two-tailed *t*-test of *P* value < 0.05 following multiple comparison correction according the Holm-Sidak method. n.d., non-determined.

Figure 6. Transcriptome analysis reveals a tight link between SUB activity and root metabolism of suberin, phenylpropanoids and cuticular lipids.

(A) Three-dimensional Principal Component Analysis (PCA) plot depicting differential transcriptome profiles of WT, *sub* and SUB-OX roots. The percentage of variance for each component appears in parentheses.

(B) Venn diagram showing genes with significantly altered expression in *sub* and SUB-OX as compared to WT roots [false discovery rate (FDR) < 0.05; $|\log_2$ fold change$|$ > 1]. The diagram indicates 392 *sub*-associated genes, 350 SUB-OX-associated genes, and 76 common genes between the two datasets. The common gene set splits to 23 genes displaying inverse expression in *sub* roots compared to SUB-OX (i.e. lower in *sub* and higher in SUB-OX or *vice versa*); and 53 genes displaying similar expression in the two genotypes (i.e. lower in both *sub* and SUB-OX or higher in both of them). Full lists of differentially expressed genes in *sub* and SUB-OX roots appear in Supplemental Tables 2 and 3, respectively.

(C) Heatmap showing the expression of 23 genes presented in [B] that display inverse expression in *sub* compared to SUB-OX roots according to their functional category.

(D) Heatmap showing the expression of 53 genes presented in [B] that display similar expression in *sub* compared to SUB-OX roots according to their functional category.

SUPPLEMENTAL DATA

Supplemental Figure 1. Common motif analysis between SUB and other Arabidopsis MYB-type transcription factors.

Supplemental Figure 2. Control assays for agroinfiltration assay.

Supplemental Figure 3. GC-MS analysis of polyesters in *N. benthamiana* leaves expressing an empty vector (EV) control and non-infiltrated regions of SUB-OX plants.

Supplemental Figure 4. Upstream regions of suberin biosynthesis genes drive expression of GUS in the Arabidopsis root endodermis.

Supplemental Figure 5. Isolation of *sub* mutant and generation of *SUB* overexpression lines.

Supplemental Figure 6. Altered endodermis suberization does not compromise Casparian strips formation in SUB-OX and *sub* roots.

Supplemental Figure 7. Vectors used in the transactivation assay.

Supplemental Figure 8. Control assay for transactivation luciferase renilla assay.

Supplemental Figure 9. Gene Ontology (GO) analysis of the 76 genes common between the differentially expressed gene datasets of *sub* and SUB-OX roots.

Supplemental Figure 10. pAtMYB9::RFP, pAtMYB107::RFP and pAtSUB::RFP promoter-reporter line expression in the Arabidopsis root.

Supplemental Table 1. Multiple statistical tests performed for elemental profiles of WT, sub and SUB-OX roots and rosette leaves.

Supplemental Table 2. List of differentially expressed genes in sub roots vs. WT following TranSeq analyses.

Supplemental Table 3. List of differentially expressed genes in SUB-OX roots vs. WT following TranSeq analyses.

Supplemental Table 4. List of oligonucleotides used for quantitative Real Time (qRT)-PCR assays and genotyping of sub mutant.

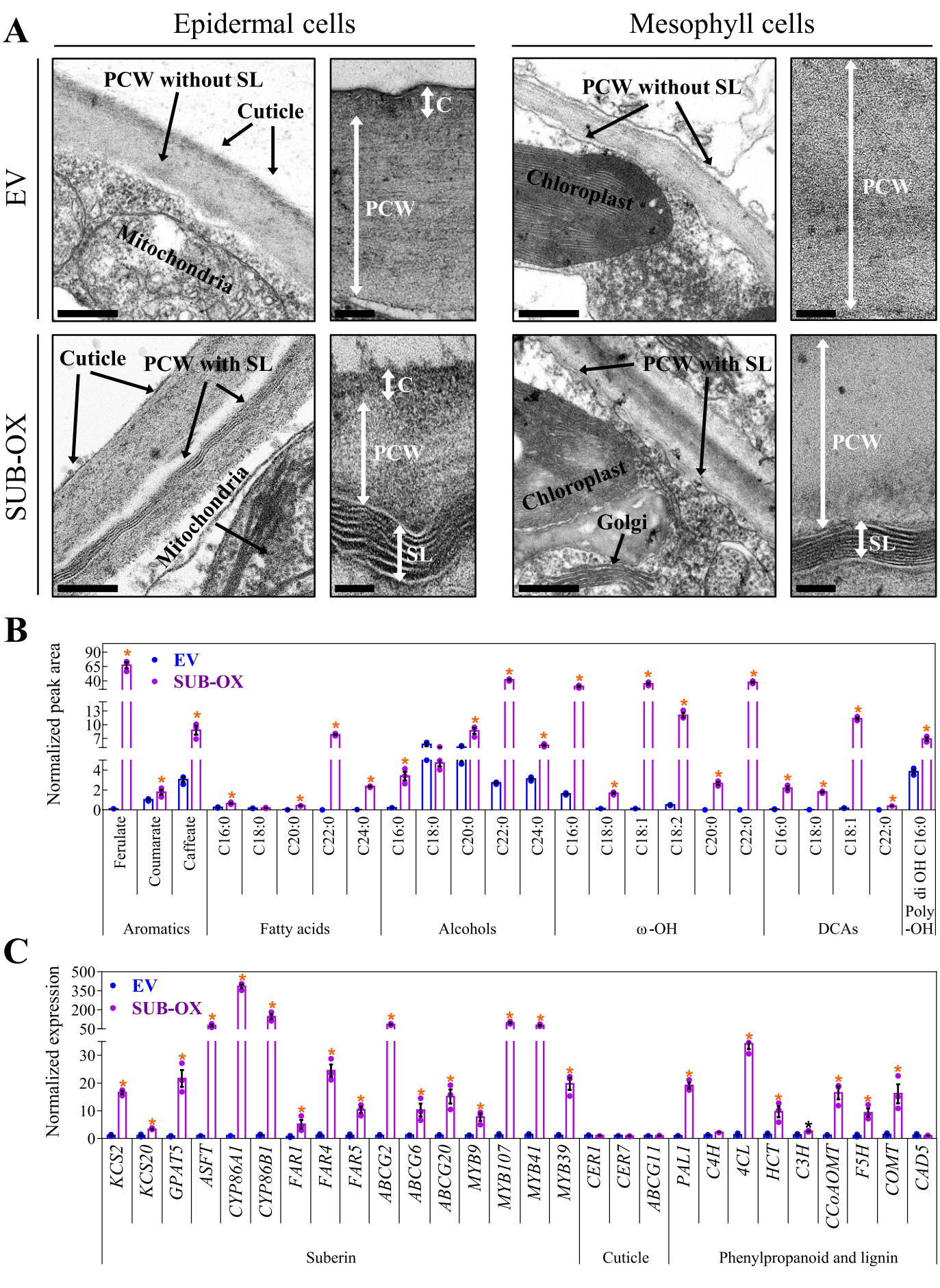
A
Epidermal cells
Mesophyll cells
EV
SUB-OX
PCW without SL
Cuticle
Mitochondria
C
PCW
Chloroplast
PCW with SL
SL
Golgi
B
Normalized peak area
EV
SUB-OX
Ferulate
Coumarate
Caffeate
C16:0
C18:0
C20:0
C22:0
C24:0
C18:1
C18:2
di OH C16:0
Aromatics
Fatty acids
Alcohols
ω-OH
DCAs
Poly -OH
C
Normalized expression
KCS2
KCS20
GPAT5
ASFT
CYP86A1
CYP86B1
FAR1
FAR4
FAR5
ABCG2
ABCG6
ABCG20
MYB9
MYB107
MYB41
MYB39
CER1
CER7
ABCG11
PAL1
C4H
4CL
HCT
C3H
CCoAOMT
F5H
COMT
CAD5
Suberin
Cuticle
Phenylpropanoid and lignin

Figure 1. Transient expression of *SUBERMAN* induces the accumulation of suberin and the deposition of suberin-like lamellae in *N. benthamiana* leaves.

(A) Transmission Electron Microscopy (TEM) images showing cell wall ultrastructure of epidermal and mesophyll cells of *N. benthamiana* leaf sections agroinfiltrated with an empty vector (EV) control or the SUB-OX vector. Bars in square micrographs represent 200 nm while those in rectangle micrographs represent 20 nm. PCW, primary cell wall; SL, suberin lamellae; C, cuticle layer. Mitochondria, chloroplasts and Golgi apparatus are marked.

(B) Leaf polyester content in *N. benthamiana* leaf sections agroinfiltrated with an EV or SUB-OX, measured by Gas Chromatography-Mass Spectrometry (GC-MS). The *y*-axis represents relative peak areas following normalization to a C_{32}-alkane internal standard. ω-OH, ω-hydroxy fatty acids; DCAs, dicarboxylic fatty acids; di-OH C16:0, 10(9),16-dihydroxy fatty acid.

(C) Expression of genes involved in the biosynthesis of suberin, cuticle, and phenylpropanoid and lignin, in *N. benthamiana* leaf sections agroinfiltrated with an EV or SUB-OX, measured by quantitative Real Time q(RT)-PCR. The *y*-axis represents relative gene expression following the normalization to endogenous constitutive *N. benthamiana* genes *PROTEIN PHOSPHATASE 2* (*PP2A*) and *F-BOX*.

Data in [B] and [C] represent mean ± s.e. of three biological replicates each generated from a pool of four infiltrated leaves and data points denote individual biological replicates. Orange asterisks indicate statistically significant differences as compared to EV determined by two-tailed *t*-test of P value < 0.05.

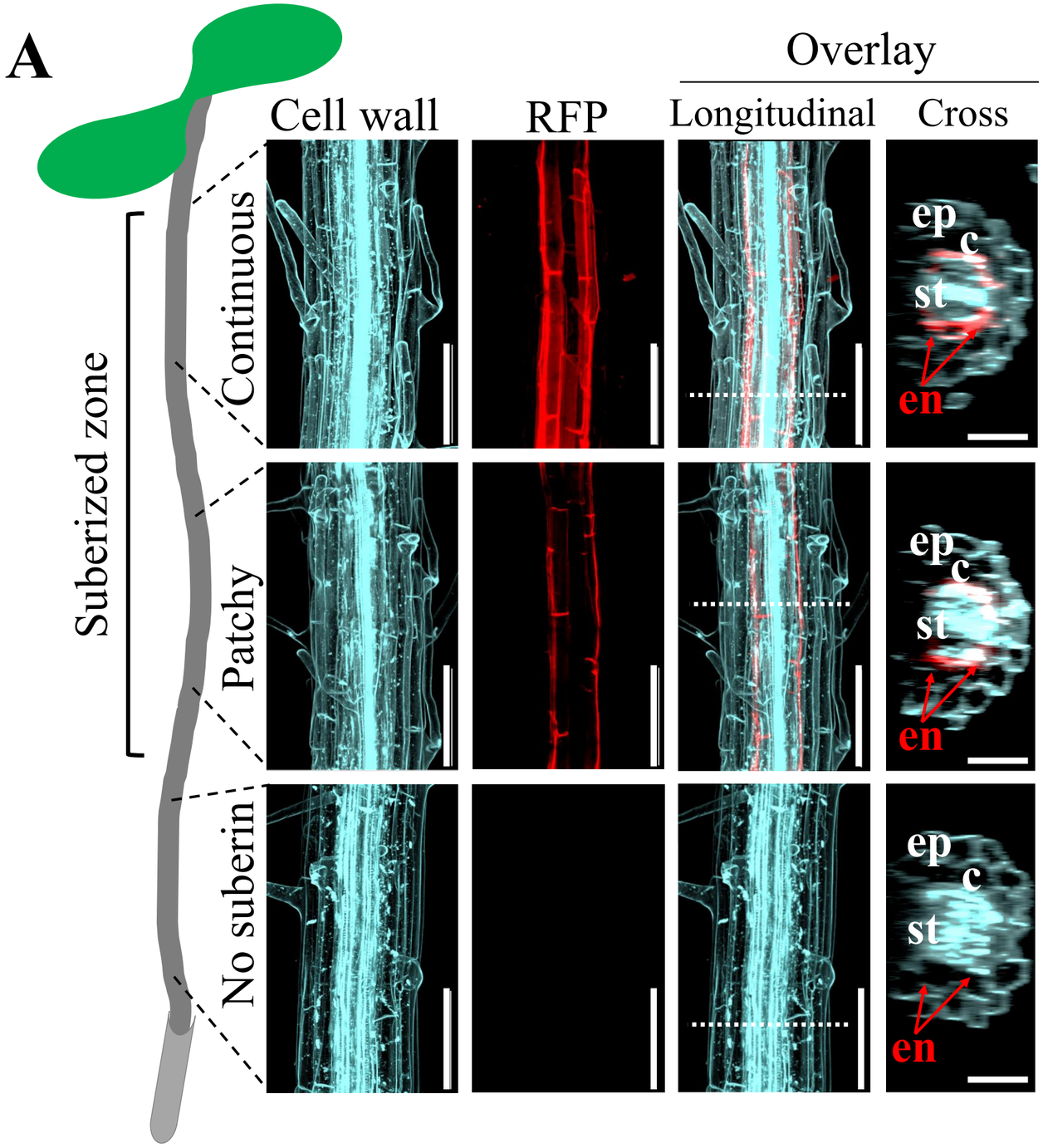
A
Overlay
Cell wall
RFP
Longitudinal
Cross
Suberized zone
Continuous
Patchy
No suberin
ep
c
st
en

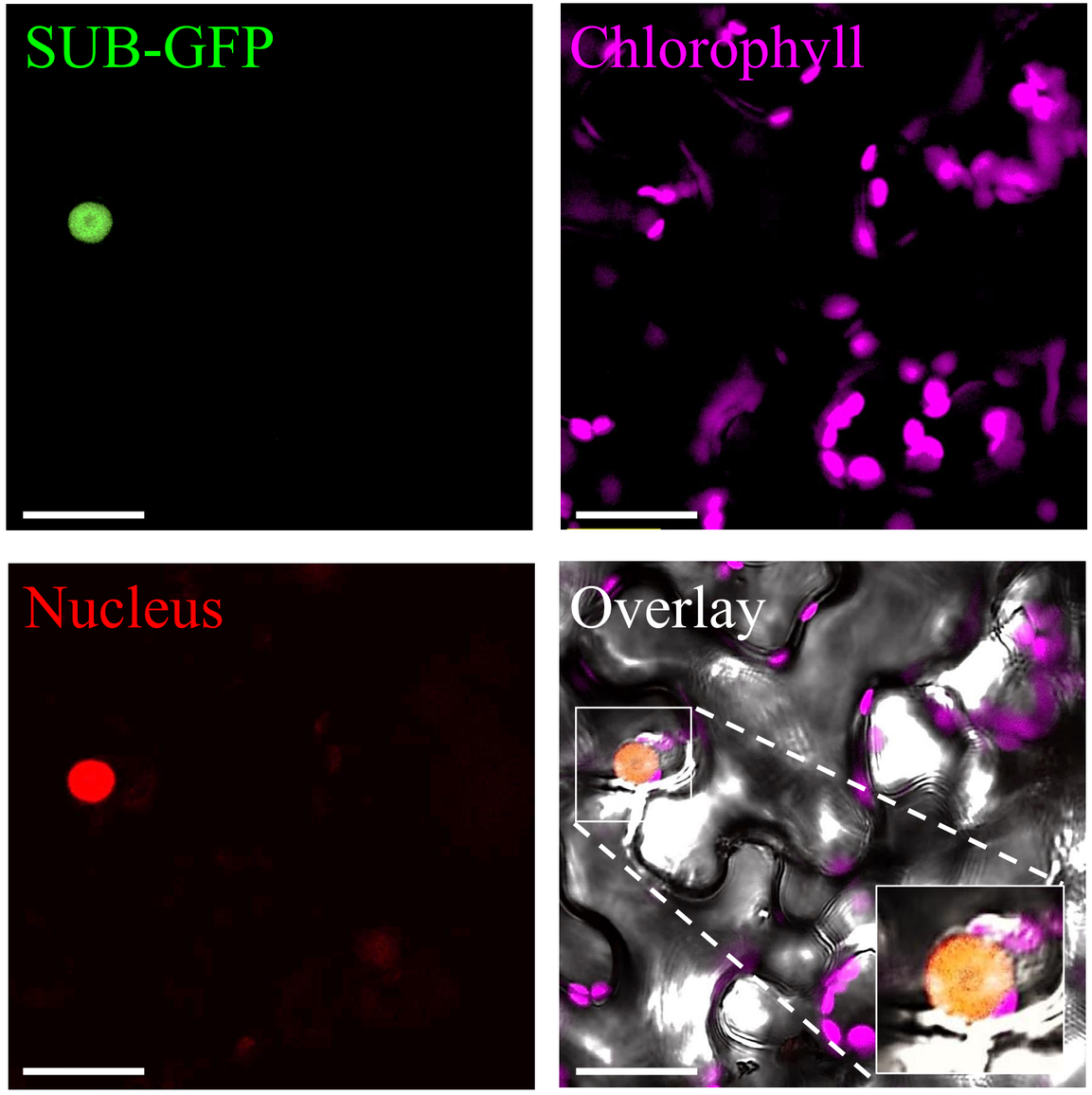
B
SUB-GFP
Chlorophyll
Nucleus
Overlay

Figure 2. *SUB* is expressed in endodermal cells displaying patchy and continuous suberization.

(A) Confocal Laser Scanning Microscopy (CLSM) images showing endodermis-specific expression of RFP driven by the native 5' upstream region of the *SUB* gene (pAtSUB::RFP) in the Arabidopsis root. Root cell layers are highlighted by Calcofluor white (cyan). Note the RFP signals (647 nm) detected in patchy and continuous suberized root zones but not in the non-suberized zone. Dashed lines in longitudinal *Z* projections represent areas of cross section views. Bars represent 50 µm.

(B) CLSM images showing nuclear localization of SUB in *N. benthamiana* leaves co-infiltrated with pSIUBQ10::AtSUB-eGFP and p35S::4xNLS-RFP vectors. Images show GFP (SUB), RFP (nucleus marker) and Cy5 (chlorophyll autofluorescence) signals. Overlay image encapsulates all three signals with bright filed. Enlarged square in the overlay image shows co-localization of GFP (SUB protein) and nuclear RFP. Bars represent 20 µm.

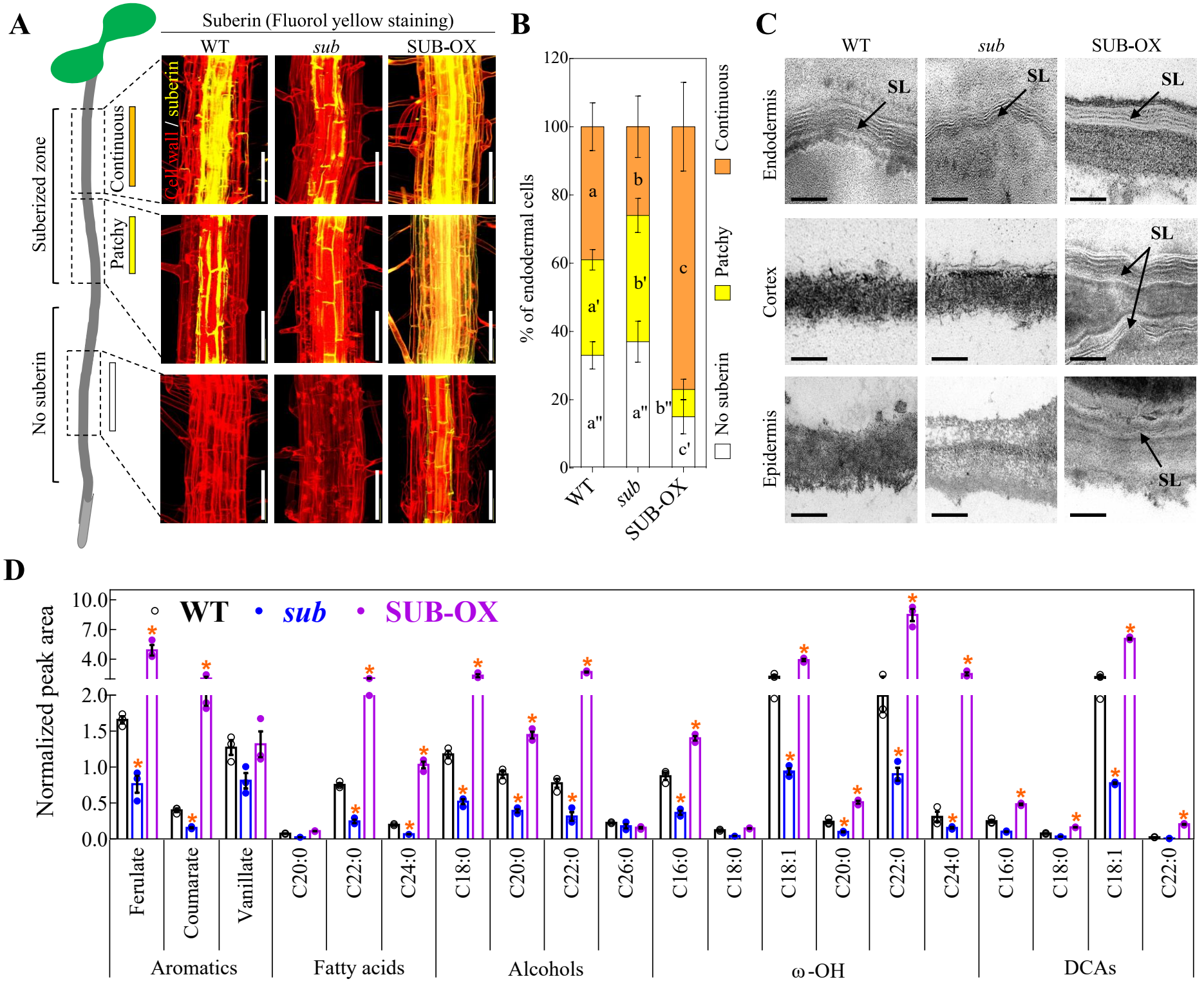
A
Suberin (Fluorol yellow staining)
WT
sub
SUB-OX
Cell wall / suberin
Suberized zone
Continuous
Patchy
No suberin
B
% of endodermal cells
Continuous
Patchy
No suberin
a
a'
a''
b
b'
a''
b''
c
c'
WT
sub
SUB-OX
C
WT
sub
SUB-OX
Endodermis
Cortex
Epidermis
SL
D
Normalized peak area
WT
sub
SUB-OX
Ferulate
Coumarate
Vanillate
C20:0
C22:0
C24:0
C18:0
C20:0
C22:0
C26:0
C16:0
C18:0
C18:1
C20:0
C22:0
C24:0
C16:0
C18:0
C18:1
C22:0
Aromatics
Fatty acids
Alcohols
ω-OH
DCAs

Figure 3. Roots with altered *SUB* expression display changes in suberin profiles.

(A) CLSM images displaying the accumulation patterns of suberin along the root axis of WT, *sub* and SUB-OX plants (*Z* projections). Root cell layers are highlighted by propidium iodide (PI; red) while suberin (yellow) was histochemically detected by FY staining. Bars represent 50 µm.

(B) Quantification of suberization degree in different zones along the root axis of WT, *sub* and SUB-OX, presented as the percentage (%) of endodermal cells. Data in bars represent means ± s.e. of ten biological replicates with small letters indicate statistically significant differences determined by one-way ANOVA of *P* value < 0.05.

(C) TEM images showing cell wall ultrastructure and suberin lamellae in epidermis, cortex and endodermis of WT, *sub* and SUB-OX roots. Images were obtained from similar regions in the continuous suberized zones from the three root genotypes. Arrows point to suberin lamellae (SL). Bars represent 40 nm.

(D) Root suberin profile measured by GC-MS. The *y*-axis represents relative peak areas following normalization to a C_{32}-alkane internal standard. Data in bars represent means ± s.e. of three biological replicates denoted by data points. Orange asterisks indicate statistically significant differences as compared to WT determined by two-tailed *t*-test of *P* value < 0.05. ω-OH, ω-hydroxy fatty acids; DCAs, dicarboxylic fatty acids.

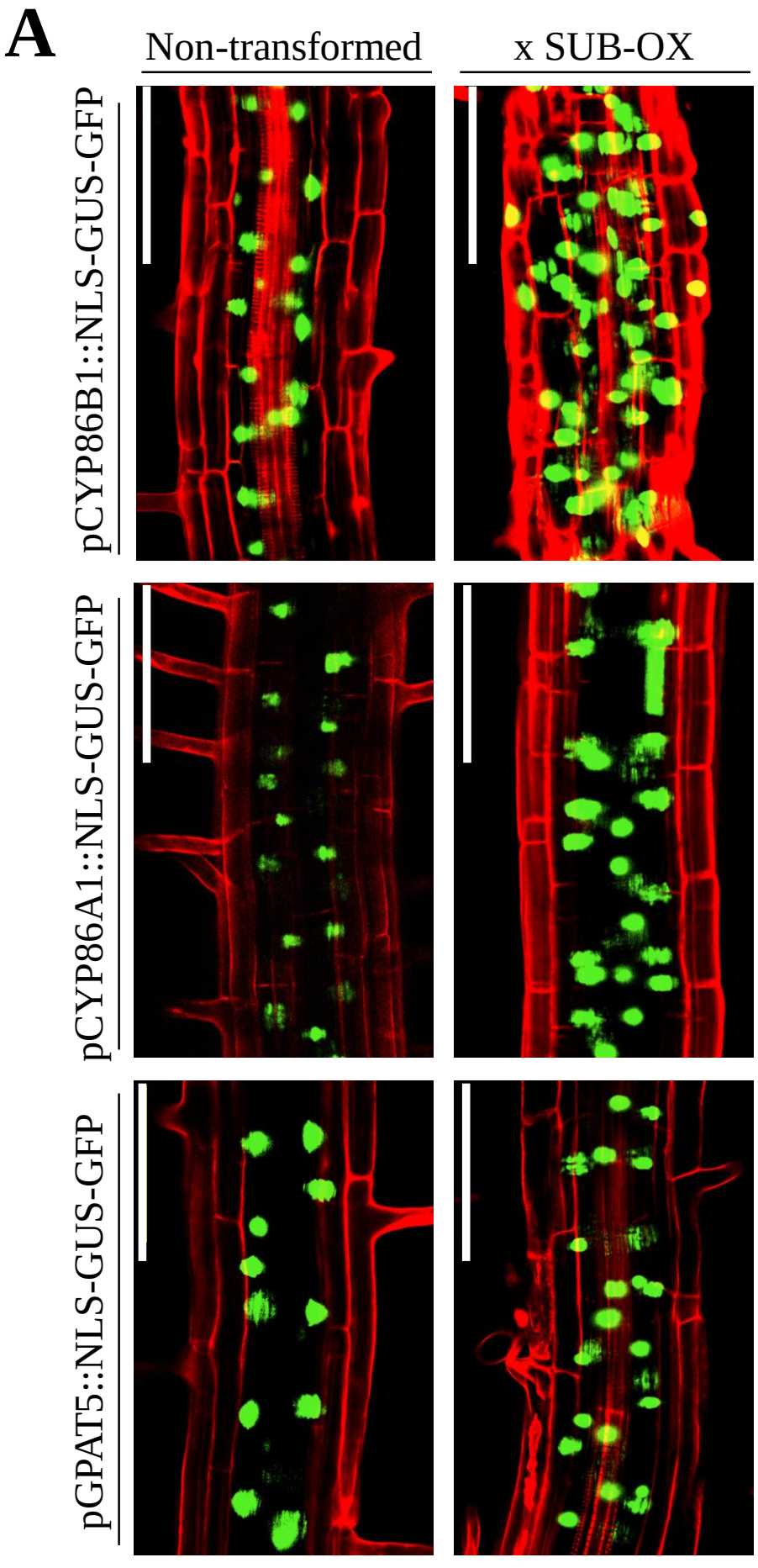
A
Non-transformed
x SUB-OX
pCYP86B1::NLS-GUS-GFP
pCYP86A1::NLS-GUS-GFP
pGPAT5::NLS-GUS-GFP

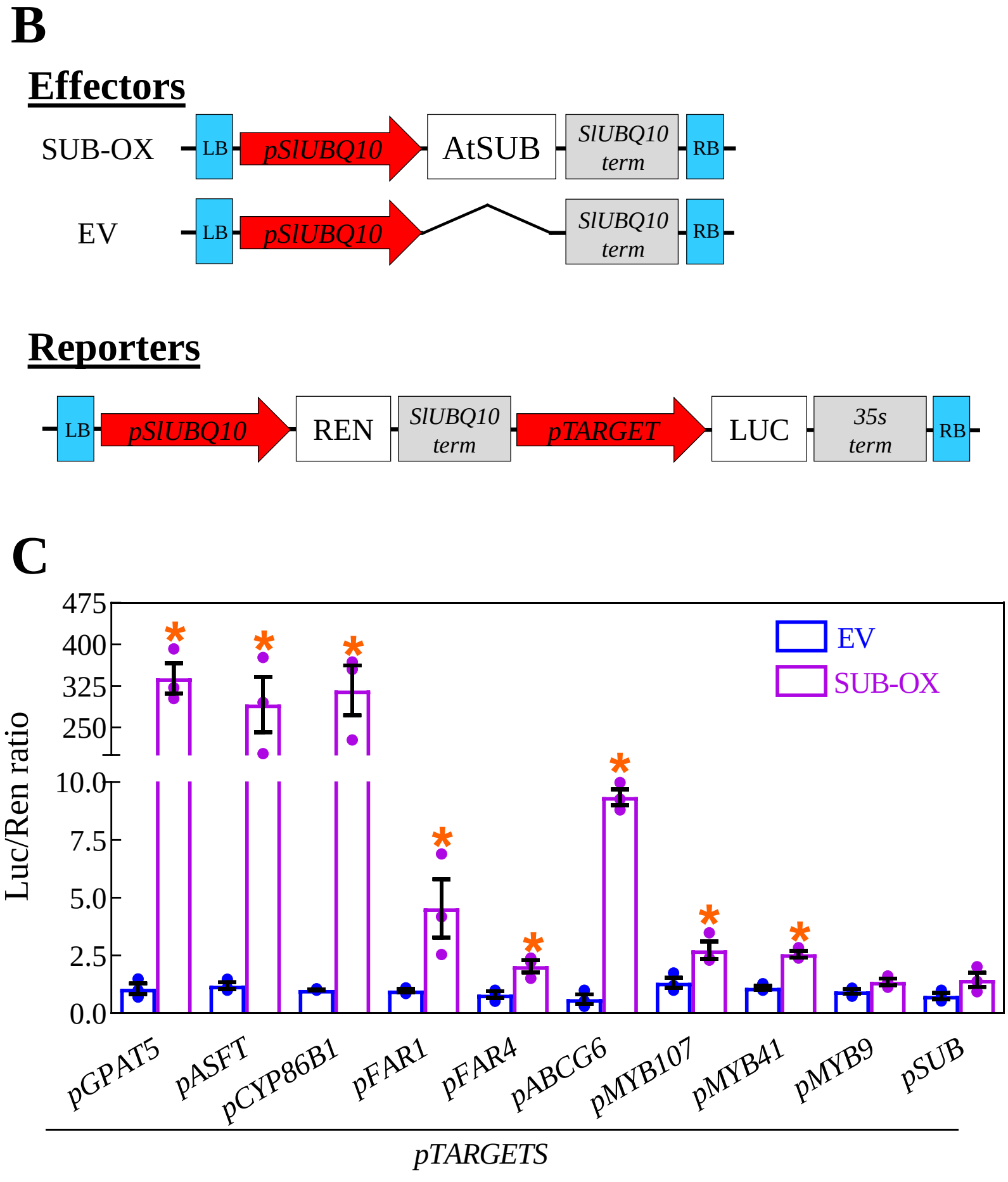
B
Effectors
SUB-OX
LB
pSlUBQ10
AtSUB
SlUBQ10 term
RB
EV
LB
pSlUBQ10
SlUBQ10 term
RB
Reporters
LB
pSlUBQ10
REN
SlUBQ10 term
pTARGET
LUC
35s term
RB
C
Luc/Ren ratio
475
400
325
250
10.0
7.5
5.0
2.5
0.0
EV
SUB-OX
pGPAT5
pASFT
pCYP86B1
pFAR1
pFAR4
pABCG6
pMYB107
pMYB41
pMYB9
pSUB
pTARGETS

Figure 4. SUB transactivates upstream regions of genes acting in suberin biosynthesis, transport and pathway regulation.

(A) CLSM images displaying the expression of GFP driven by the native 5' upstream regions of *GPAT5*, *CYP86A1* or *CYP86B1* genes in continuous suberized root zones of pGPAT5::NLS-GFP-GUS, pCYP86A1::NLS-GFP-GUS and pCYP86B1::NLS-GFP-GUS reporter lines non-transformed or ones transformed with SUB-OX. Root cell layers are highlighted by PI staining (red). Bars represent 50 µm.

(B) Diagrams of effector and reporter vectors used for the transactivation luciferase assay depicted in [C]. Full names of all genes and controls used in this assay are listed in Supplemental Figure 7.

(C) Transactivation luciferase assay measuring the capacity of the SUB transcription factor to induce upstream regions in the promoter regions of suberin genes. The *y*-axis represents fold changes of *luciferase* (Luc) to *renilla* (Ren) rations between SUB-OX as compared to EV. Data in bars represent mean ± s.e. of four biological replicates each generated from a pool of four infiltrated leaves and data points denote individual biological replicates. Orange asterisks indicate statistically significant differences as compared to EV determined by two-tailed *t*-test of *P* value < 0.05.

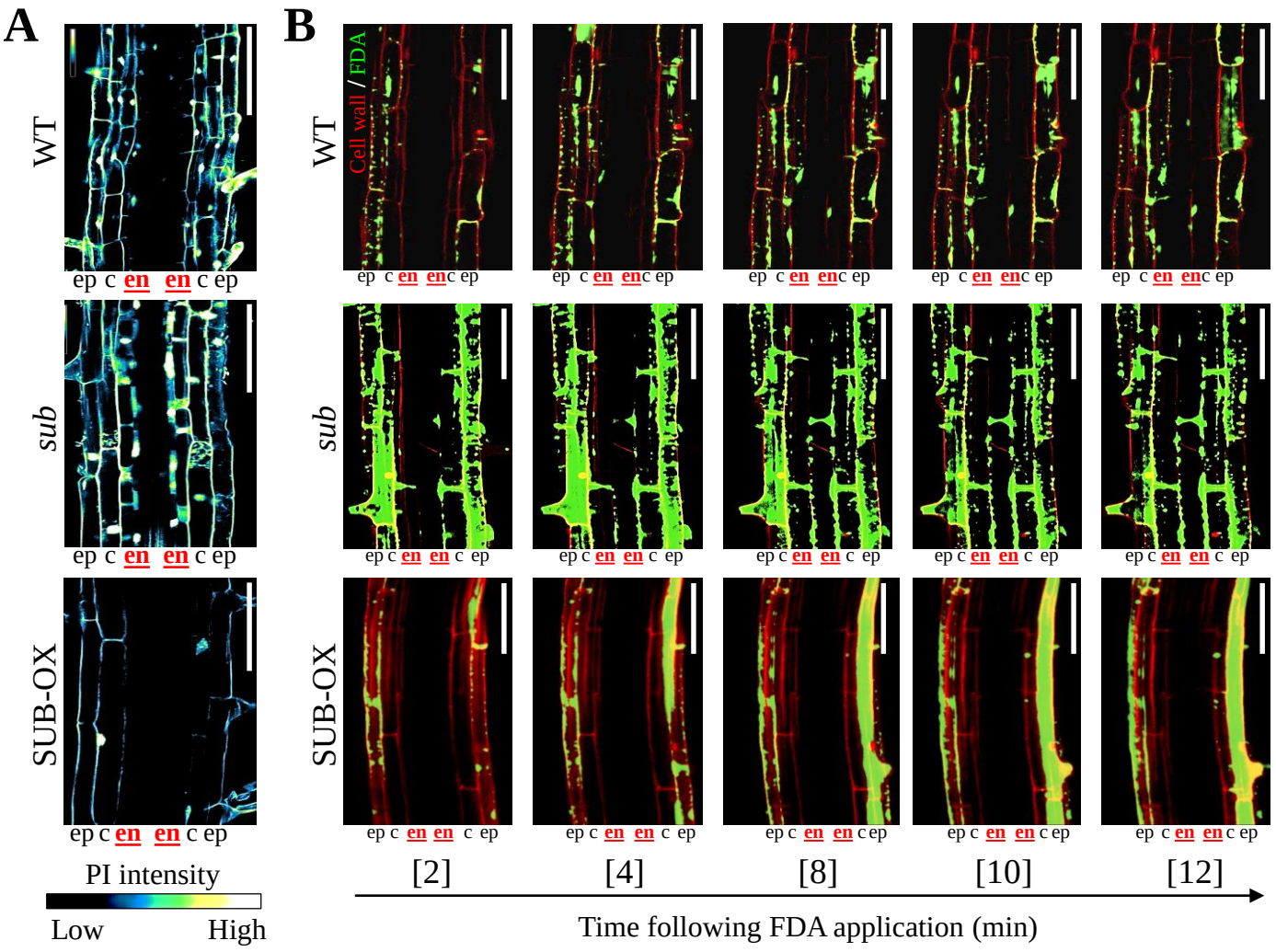

C

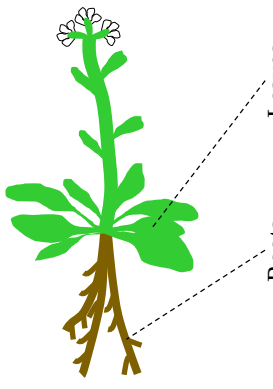

	Li	B	Na	Mg	P	S	K	Ca	Mn	Fe	Co	Ni	Cu	Zn	As	Se	Rb	Sr	Mo	Cd
Leaves *sub*					*		*					n.d.				n.d.	*	*		n.d.
Leaves SUB-OX	*			*	*	*	*	*	*	*	*	n.d.	*			n.d.	*	*		n.d.
Roots *sub*											* n.d.	n.d.				n.d.				n.d.
Roots SUB-OX				*			*			*		n.d.				n.d.				n.d.

0.14 2.33
Fold-change vs. WT

Figure 5. Alterations in endodermis suberin lamellae affect root uptake capacities.

(A) CLSM images displaying PI penetration across cell layers of WT, *sub* and SUB-OX roots. Images were taken from similar parts of continuous suberized zones of all three genotypes 5 minutes following PI application. Bars represent 75 µm. ep, epidermis; c, cortex; en, endodermis.

(B) CLSM images showing fluorescein diacetate (FDA) penetration across cell layers of WT, *sub* and SUB-OX roots. Representative images were taken from similar parts of continuous suberized zones of all three genotypes 2 to 12 minutes following FDA application in 2 minutes intervals. Bars represent 50 µm. ep, epidermis; c, cortex; en, endodermis.

(C) Elemental composition analysis performed in roots and rosette leaves harvested from WT, *sub* and SUB-OX 3-week-old plants. Elements were determined by Inductively Coupled Plasma-Mass Spectrometry (ICP-MS) analysis. The heatmap represents the fold-change of each element per tissue compared to the corresponding WT tissue. Red asterisks indicate statistically significant differences as compared to WT determined by two-tailed *t*-test of *P* value < 0.05 following multiple comparison correction according the Holm-Sidak method. n.d., non-determined.

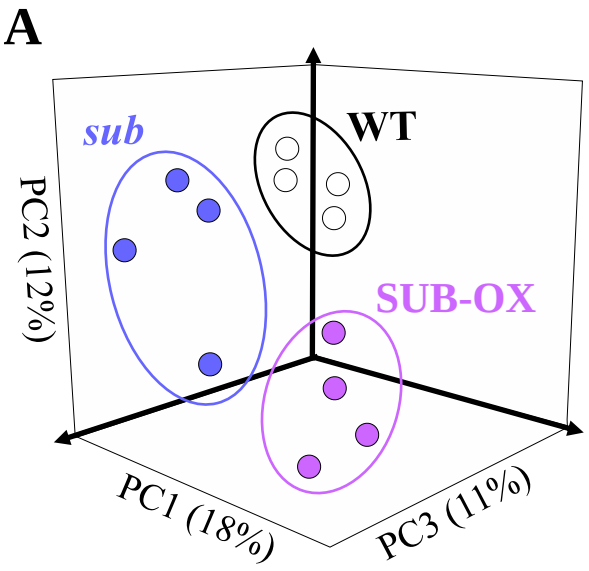

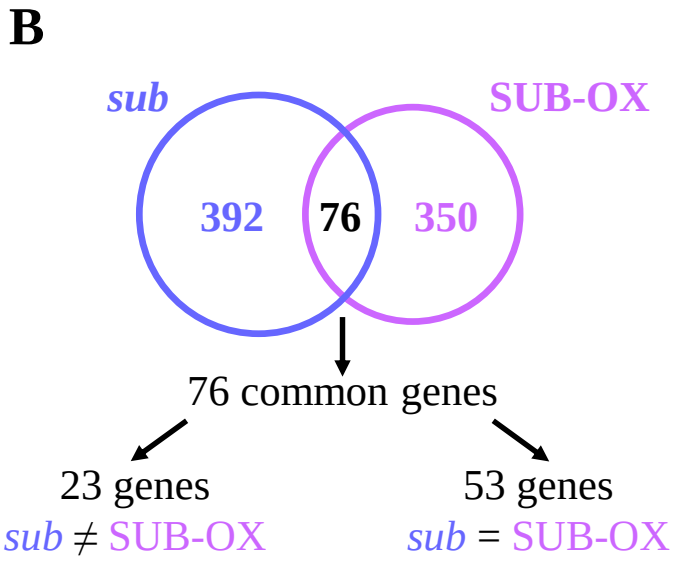

C 23 genes *sub* ≠ SUB-OX

Function	Gene ID	*sub*	SUB-OX
Suberin	*KCS2*		
	GPAT5		
	ASFT		
	CYP86A1		
	CYP86B1		
	FAR1		
	FAR4		
	FAR5		
	ABCG2		
	ABCG6		
	ABCG20		
	MYB41		
	SUBERMAN		
Lignin	*LAC5*		
Lipid and wax	*Pollen Ole e 1*		
	CYP86A2		
Unknown	*Unknown protein*		
	Unknown protein		
	Unknown protein		
	Unknown protein		
	Unknown protein		
	Unknown protein		
	Unknown protein		

Log$_2$ fold-change vs. WT

Low — High

D 53 genes *sub* = SUB-OX

Function	Gene ID	*sub*	SUB-OX
Cell wall	*AGP30*		
	XTH24		
	Putative lipoprotein		
Ion transport	*SULTR3;5*		
	ALMT1		
	HAK5		
	IRT1		
	DEFL		
	Transmembrane protein		
	YSL3		
Phosphate	*IPS1*		
	IPS2		
	PS2		
	PS3		
	SPX1		
	SPX3		
	GDPD1		
	PAP17		
	PEPC1		
	PHT1;4		
	HHO1		
Photosynthesis	*LHCB1.3*		
	LHCB3		
IAA signaling	*SAUR72*		
	DAO2		
ABA signaling	*CAR8*		

Function	Gene ID	*sub*	SUB-OX
Lignin	*PRX52*		
Lipid	*LTP*		
Carbohydrates	*QQS*		
	Lectin protein		
Asparagine	*ASPGB1*		
Sulfolipids	*SQD1*		
	SQD2		
Thalianols	*THAD1*		
	THAH1		
Oxidoreduction	*GST1*		
	Rossmann-fold protein		
	Peroxidase protein		
	Peroxidase protein		
Phosphorylation	*HAD protein*		
	DSP1		
	Phosphorylase protein		
Defence	*NHL10*		
Mitochondria	*Cox19-like CHCH protein*		
Chloroplast	*SPD1*		
Unknown	*Unknown protein*		
	Unknown protein		
	Unknown protein		
	Unknown protein		
	Unknown protein		
	Unknown protein		
	Unknown protein		
	Unknown protein		

Figure 6. Transcriptome analysis reveals a tight link between SUB activity and root metabolism of suberin, phenylpropanoids and cuticular lipids.

(A) Three-dimensional Principal Component Analysis (PCA) plot depicting differential transcriptome profiles of WT, *sub* and SUB-OX roots. The percentage of variance for each component appears in parentheses.

(B) Venn diagram showing genes with significantly altered expression in *sub* and SUB-OX as compared to WT roots [false discovery rate (FDR) < 0.05; $|\log_2$ fold change| > 1]. The diagram indicates 392 *sub*-associated genes, 350 SUB-OX-associated genes, and 76 common genes between the two datasets. The common gene set splits to 23 genes displaying inverse expression in *sub* roots compared to SUB-OX (i.e. lower in *sub* and higher in SUB-OX or *vice versa*); and 53 genes displaying similar expression in the two genotypes (i.e. lower in both *sub* and SUB-OX or higher in both of them). Full lists of differentially expressed genes in *sub* and SUB-OX roots appear in Supplemental Tables 2 and 3, respectively.

(C) Heatmap showing the expression of 23 genes presented in [B] that display inverse expression in *sub* compared to SUB-OX roots according to their functional category.

(D) Heatmap showing the expression of 53 genes presented in [B] that display similar expression in *sub* compared to SUB-OX roots according to their functional category.